Journal of Materials Chemistry B

Accepted Manuscript

ROYAL SOCIETY OF CHEMISTRY

www.rsc.org/materialsB

Table of Contents Graphic

Enzymatic Degradation of Oxidized and Reduced Graphene Nanoribbons by Lignin Peroxidase

Gaurav Lalwani[#], Weiliang Xing[#] and Balaji Sitharaman[*]

Department of Biomedical Engineering, Stony Brook University, Stony Brook, NY 11794-5281

# These authors contributed equally to the work

*Correspondence:
Balaji Sitharaman, Ph.D.
Department of Biomedical Engineering
Bioengineering Building Room 115
Stony Brook University
Stony Brook, NY 11794-5281
Tel: 631-632-1810
Email: balaji.sitharaman@stonybrook.edu

Graphic:

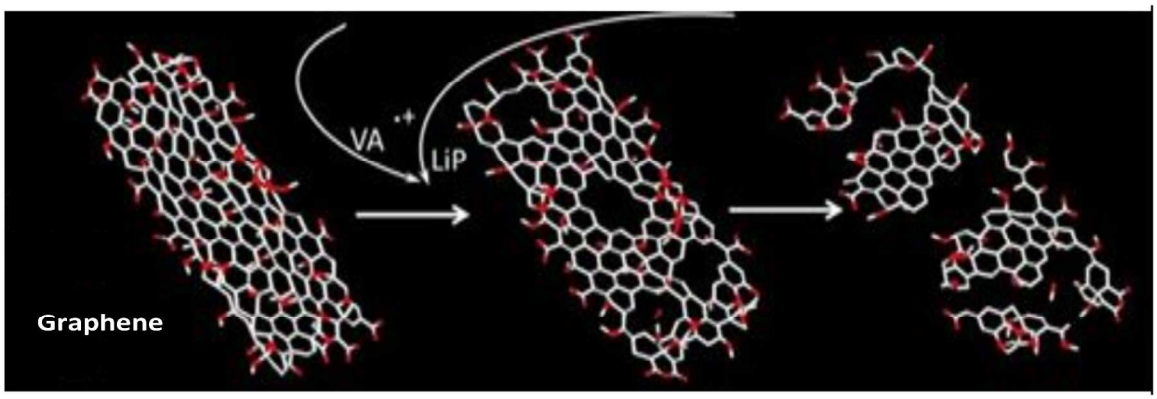

We report structural degradation of oxidized and reduced graphene nanoribbons by the enzyme lignin peroxidase

Enzymatic Degradation of Oxidized and Reduced Graphene Nanoribbons by Lignin Peroxidase

Gaurav Lalwani[#], Weiliang Xing[#] and Balaji Sitharaman[*]

Department of Biomedical Engineering, Stony Brook University, Stony Brook, NY 11794-5281

# These authors contributed equally to the work

*Correspondence:
Balaji Sitharaman, Ph.D.
Department of Biomedical Engineering
Bioengineering Building Room 115
Stony Brook University
Stony Brook, NY 11794-5281
Tel: 631-632-1810
Email: balaji.sitharaman@stonybrook.edu

Abstract:

The expanding use of graphene for various industrial and biomedical applications requires efficient remediation strategies during their disposal into waste streams. Additionally, the interactions of graphene with the biota need thorough evaluation. In this study, we investigated the interactions of oxidized and reduced graphene oxide nanoribbons (GONRs and rGONRs) with lignin peroxidase (LiP), a ligninolytic enzyme released from white rot fungus. GONRs and rGONRs were treated with LiP in the presence and absence of veratryl alcohol (VA; an electron transfer mediator and secondary metabolite of white rot fungi). Transmission electron microscopy showed the formation of large defects (holes) in the graphene sheet, which increased in diameter with increased degradation time. Raman spectroscopic analysis indicated that, within 96 hours, in the presence of hydrogen peroxide and VA, the GONRs and rGONRs were completely and partially degraded by LiP, respectively. Comparisons between groups with or without VA showed that degradation of GONRs was accelerated in the presence of VA. These results indicated that LiP could efficiently degrade GONRs and rGONRs in the presence of VA, suggesting that VA may be an essential factor needed to degrade rGONRs via LiP treatment. Thus, the wide presence of white rot fungi, and thereby LiP, in nature, could lead to efficient degradation of graphene present in the environment. Additionally, LiP, which has a higher theoretical redox potential compared to horseradish peroxidases and myeloperoxidases, could be a better candidate for the environmental remediation of graphene.

Key words: Lignin peroxidase, graphene oxide, reduced graphene oxide, degradation, enzymatic oxidation

1. Introduction:

The excellent physiochemical properties of the two-dimensional carbon nanostructure graphene, [1, 2] could allow high impact applications in material [3-6] and biomedical sciences [7-18]. Depending on the application, pristine graphene and graphene oxide (GO) have been employed. Pristine graphene is routinely synthesized by micromechanical exfoliation, epitaxial growth, or chemical vapor deposition, while GO can be synthesized by Hummer's method followed by exfoliation, or longitudinal unzipping of carbon nanotubes [19]. GO typically possesses sub-optimal electrical conductivity (due to disruption of sp^2 bonds), and has been subjected to reduction (to restore sp^2 bonds and improve its electrical conductivity) by physical (thermal annealing) and chemical (hydrazine, metal hydrides, and hydrohalic acids) methods [20].

The long-term (months and years) impact of graphene, GO, and rGO on the environment and human health remains unknown, and there exist numerous contradictory reports on their short-term (days and weeks) biocompatibility and environmental toxicology [21-27]. Several studies have reported structural degradation of carbon nanotubes and graphene upon interaction with strong oxidants (hydrogen peroxide [H_2O_2], sodium hypochlorite, etc.) and acids (sulfuric acid, nitric acid, etc.) [28-31]. However, these methods have limited practical applications. The use of strong acids and oxidants can have harmful unpredicted effects on flora and fauna; therefore, these strategies cannot be used to degrade carbon nanomaterials present or released into the environment. Recently, studies using the peroxidase family of enzymes, such as horseradish peroxidases (HRP) and myeloperoxidases (MPO), to degrade graphene oxide [32] and single- and multi-walled carbon nanotubes (SWCNTs and MWCNTs, respectively) *in vitro* and *in vivo* [28, 29, 33-37] have highlighted the importance of an eco-friendly enzymatic degradation strategy for carbon nanomaterials. However, these methods possess several limitations, such as

low degradation efficiency (enzymatic treatment may last up to 60 days [28]) and the dependence on substrate chemistry (for example, reduced graphene oxide nanoribbons [rGONRs] failed to be degraded by HRP [32]), impeding their practical use. Due to these limitations, improvements in the development of eco-friendly green strategies for the degradation of oxidized and reduced carbon nanomaterials remains an active area of research.

White rot fungi (*Phanerochaete chrysosporium*) are ubiquitous, naturally occurring organisms distributed worldwide, especially in forest soils with decaying woody matter. Lignin peroxidase (LiP) is a ligninolytic enzyme released from white rot fungi, responsible for the degradation of lignin, a matrix component surrounding cellulose in plant cell walls. It has been shown that LiP can cleave the aromatic rings of complex polymers, such as lignin, and other organic molecules such as DDT (dichloro-diphenyl-trichloroethane) and PCBs (polychlorinated biphenyls), leading to the formation of oxidized side chains and aromatic residues [38, 39]. During these oxidation reactions, VA (veratryl alcohol; a fungal metabolite released by white rot fungi) functions as a free radical mediator, assisting the electron transfer between LiP and the substrate. The VA cation radical formed during this process can directly oxidize chemicals that are not oxidized by LiP [40]. LiP has greater redox potential than HRP and MPO [41-43], and, when coupled with VA, possesses significantly higher enzymatic activity [40, 44]. Thus, given the widespread presence of LiP, and the potential use of graphene for several technological and commercial applications, in this study, we investigated the interactions of GONRs and rGONRs with LiP in the presence and absence of VA.

2. Materials and methods:

2.1 Materials:

Lignin peroxidase, hydrogen peroxide (3%), 3,4-dimethoxybenzyl alcohol (veratryl alcohol [VA]), sodium L-tartrate dibasic dehydrate, and L-(+)-tartaric acid were purchased from Sigma Aldrich® (New York, USA). GONRs were synthesized by longitudinal unzipping of MWCNTs (Sigma Aldrich, NY, USA, Cat. No. 659258) and were reduced with hydrazine to form rGONRs as described previously [45, 46].

2.2 Enzymatic kinetic assay:

LiP activity in the presence and absence of GONRs was determined at 310 nm using an Evolution 300 UV-Vis Spectrophotometer (Thermo scientific®, West Palm Beach, FL, USA) as follows: 4.2 mM of VA was incubated with 7.5 µg/ml LiP with or without 0.75 mg/ml GONRs. The reaction mixture was made up to a final volume of 1 ml by adding 0.42 mM H_2O_2 to start the reaction. The assays were carried out at 23°C, the optimal temperature for LiP activity [47]. Data is reported in international units (U/I), with one unit (U) of LiP activity defined as one µmol of VA oxidized in one minute. The data in Figure 1 (H) were fitted with an exponential plot using MatLab (MathWorks®, Natick, MA, USA). The absorbance was normalized to the baseline absorbance of 4.2 mM VA solution prior to the addition of LiP and GONRs.

2.3 Degradation of GONRs and rGONRs:

The various experimental and control groups are listed in Figure 1 B-E. Briefly, 0.5 ml of 2.5 mg/ml GONRs and rGONRs were dispersed in 10× buffer solution (2.5 mmol tartaric acid and 7.5 mmol sodium L-tartrate dibasic dehydrate, pH=3.05). The solutions were subjected to bath

sonication (1 hour, Ultrasonicator FS30H, Fischer Scientific, Pittsburgh, PA, USA) to generate stable suspensions. To these suspensions, VA (0.5 ml of 6.359 µl/ml), LiP (3 ml, 0.25 mg/ml), and 3% H_2O_2 were added. All vials were filled up to total volume of 10 ml with buffer, and sealed with a septum. The final concentrations of VA and H_2O_2 in the vials were 4.2 mM and 0.42 mM, respectively, which are the optimal concentrations for lignin peroxidase activity [47]. H_2O_2 was used to initiate the reaction. After every 15-minute time interval, 6 µl of 70 mM H_2O_2 and/or 4 µl of 15 mg/ml LiP were added to the reaction vials using a needle through the septum. H_2O_2 and/or LiP were replenished after every 15 minutes to continue the reaction for a total period of 96 hours. All vials were stirred continuously at 300 rpm at 23°C in the dark.

2.4 Transmission electron microscopy (TEM):

GONRs and rGONRs were collected and centrifuged at 3400 rpm for 30 min to eliminate salt contributions from the buffer. The collected pellet was mixed with 1:1 DI water:ethanol, probe sonicated for 1 minute using a 1 sec 'on' 2 sec 'off' cycle (LPX 750 Ultrasonicator, Cole Parmer, IL, USA), and centrifuged at 3000 rpm for 5 minutes. The resulting supernatant was dropped on to TEM grids (300 mesh size, lacey carbon grids on a copper support; Ted Pella Inc., Redding, CA, USA) and dried overnight. TEM imaging was performed using an FEI Tecnai^{TM} BioTwinG^2 transmission electron microscope at an accelerating voltage of 80 kV. Digital images were acquired using an AMT XR-60 CCD digital camera system.

2.5 Raman spectroscopy:

Samples for Raman spectroscopy were prepared by drop casting 20 µl of GONR or rGONR sample after every 4-hour time interval on a silicon wafer (TED Pella®, Redding, CA, USA) and air-dried. Point spectra were collected using a µSense Raman Microscope (Enwave optronics®,

Irvine, CA, USA) at 532 nm. Spectra were collected 5 times per location for 15 locations per sample and averaged.

3. Results:

3.1 Enzyme kinetics assay:

During LiP-mediated oxidation, VA functions as a free radical mediator, assisting the electron transfer between LiP and the substrate. The VA cation radical formed during this process has been shown to directly oxidize substrates [40]. Therefore, to measure the activity of LiP in the presence and absence of GONRs, LiP was incubated with VA and GONRs at 23°C. The enzymatic activity assay showed that the consumption of VA accelerated in the presence of GONRs, limiting the reaction time to 15 minutes (Figure 1 A).

3.2 Gross visual observation:

Figure 1 B-E shows the optical images of the experimental and control group vials with or without LiP, VA, or H_2O_2 after 0 and 96 hours of incubation. The vials in Figure 1 B and D contain GONRs, and those in C and E contain rGONRs. Figure 1 D shows the vial containing LiP, VA, and H_2O_2 (vial I) to be more transparent than the one without VA (vial II). The control groups in vials III and IV (Figure 1 B and D), which did not contain H_2O_2 and LiP, respectively, did not show any change color. For the rGONRs (Figures 1 C and E), vials containing LiP, H_2O_2, and VA (vial I) showed a noticeable color change, compared to the other three vials (vials II, III, and IV), although the change of color in these vials was not as pronounced compared to the vials with GONRs (nearly transparent; Figure 1 D, vial I). No noticeable differences were observed between the other three vials (Figure 1 E; vials II, III, and IV, lacking VA, H_2O_2 and LiP, respectively).

3.3 Transmission electron microscopy:

TEM was performed to characterize the structural degradation of GONRs and rGONRs. Figure 2 shows representative TEM images of GONRs (Figure 2 A-D) and rGONRs (Figure 2 E-H) at various time points (0, 4, 48, 72, and 96 hours) treated with LiP, VA, and H_2O_2. Pristine GONRs (Figure 2 A) and rGONRs (Figure 2 E) were present as flat, smooth, and uniform multi-layered sheets of graphene without any structural defects. After 4 hours, the GONRs showed noticeable wrinkles (Figure 2 B, black arrows), and numerous holes (Figure 2 B, nanoribbon area marked with yellow circle) with an average diameter of 13.5 ± 7.0 nm were observed. Conversely, few or no holes were observed in the rGONR structure (Figure 2 F, black arrow) after 4 hours of LiP treatment. After 48 hours, large holes (up to 320 nm diameter, Figure 2 D) were observed in the GONRs, leading to disruption of the nanoribbon structure. Several small holes (Figure 2 H, black arrows) and cleavages of nanoribbon architecture (Figure S1) were observed in the rGONRs after 48 and 72 hours of treatment, respectively. After 96 hours, the GONR structure was degraded, and amorphous carbonaceous aggregates (Figure 2 D) were observed. Holes extending from the outer to inner layers of the rGONR sheets were also present (Figure 2 H).

Figures S2 and S3 display the morphology of the GONRs and rGONRs treated with LiP and H_2O_2 in the absence of VA. Similar to in Figure 2 A and E, the pristine GONRs and rGONRs appeared as flat and smooth nanoribbons without any structural defects. Incubation of GONRs with LiP and VA for 48 hours resulted in the formation of small holes (Figure S2 C), which increased in diameter after 72 hours (Figure S2 D). Formation of holes in GONRs in the presence of LiP and VA began after 48 hours of incubation (Figure S2 C, black arrows),

suggesting that the degradation process is slower in the absence of VA. Large holes (~ 50 nm diameter) were observed after 96 hours of treatment of GONRs. Figure S3 A and B shows the morphology of rGONRs incubated with LiP and H_2O_2 after 0 and 96 hours. No structural degradation of the rGONRs was observed even after 96 hours of incubation.

3.4 Raman spectroscopy:

Raman spectroscopy was used to characterize the perturbations (chemical changes, structural defects) on the GONRs and rGONRs caused by their interactions with LiP and other cofactors (VA, H_2O_2). Figure 3 shows Raman spectra of GONRs treated with LiP, VA, and H_2O_2 (Figure 3 A); GONRs treated with LiP and H_2O_2 (Figure 3 B); rGONRs treated with LiP, VA, and H_2O_2 (Figure 3 C); and rGONRs treated with LiP and H_2O_2 (Figure 3 D). Characteristic Raman peaks were observed at 1370 cm^{-1} (D band) and at 1600 cm^{-1} (G band) [48]. Changes in the intensities of the D and G bands were also observed at various time points. Table 1 lists the I_D/I_G ratios after 0, 24, 72, and 96 hours of treatment. For GONRs treated with LiP, VA, and H_2O_2 (Figure 3 A, E), the I_D/I_G ratio increased from 1.32 at the beginning of degradation to 1.89 after 96 hours of treatment. At the end of the degradation, both the D and G band disappeared. The second vial, in which GONRs were exposed to LiP and H_2O_2, but not VA (Figure 3 B, F), showed an increase in the I_D/I_G ratio from 1.32 at 0 hours to 1.64 after 72 hours followed by a decrease to 1.49 at the end of degradation process (Table 1). Figure 3 C and G shows the changes in the D and G bands intensities of rGONRs exposed to LiP in the presence of VA. The I_D/I_G ratio increased from 1.51 (0 hours) to 1.77 (96 hours). Figure 3 D and H shows the I_D/I_G ratio of rGONRs exposed to LiP

in the absence of VA. The I_D/I_G ratio increased from 1.51 to 1.81 after 24 hours, followed by a decrease to 1.70 after 96 hours of LiP treatment.

3.5 Quantification of structural defects:

To further investigate the structural morphology, we measured the diameter of the holes (D in nm, inset Figure 4) and the distance between two holes (d in nm) after degradation of the GONRs and rGONRs with LiP in the presence of VA and H_2O_2. Figure 4 A shows the distribution of the diameter of the holes in the GONRs after 4 and 48 hours of enzymatic treatment. The diameter of the holes were between 5-20 nm after 4 hours, and increased to ~320 nm after 48 hours. Furthermore, the distance between holes (Figure 4 B) ranged between 5-145 nm after 4 hours, and increased to ~310 nm after 48 hours of treatment. For rGONRs, the diameter of the holes (Figure 4 C) increased from 5-30 nm after 48 hours to ~205 nm after 96 hours of treatment. The distance between the holes (Figure 4 D) was between 5-180 nm after 48 hours, and decreased to 5-70 nm after 96 hours, suggesting an increase in the density of holes on the rGONRs after 96 hours. The only difference between the degradation of GONRs and rGONRs was the delayed occurrence of hole formation in the rGONRs, which was observed at the 48-hour time point compared to the GONRs, which showed holes at the 4-hour time point.

Discussions:

The objective of this study was to assess and evaluate the interactions of GONRs and rGONRs with LiP. Towards this end, GONRs and rGONRs were incubated with LiP and H_2O_2 (in the presence and absence of VA), and structural degradation was monitored using Raman spectroscopy and TEM image analysis. The various experimental and control groups are listed in Figure 1 B-E.

LiP activity can be analyzed by measuring the oxidation of VA [47]. During LiP mediated oxidation, the VA cation radical can directly oxidize substrates [40] (graphene in our study), thereby accelerating the consumption of LiP in the reaction. Therefore, we measured the consumption of VA as a measure of LiP activity in the presence and absence of GONRs (Figure 1 A). Our results show that, in the presence of GONRs, H_2O_2, and LiP, the consumption of VA is accelerated. H_2O_2 is thermodynamically unstable at room temperature and spontaneously degrades to form water and oxygen. Therefore, experiments were designed wherein H_2O_2 was added at 15 minutes time intervals. Previous reports have shown that a low pH value (pH = 3.05 in our experiments — the optimal pH value for the reaction in the presence of LiP) decreases the temporal stability of the enzyme, and lowers the longevity of enzymatic activity [49]. Therefore, LiP was also added to the reaction mixture at 15-minute intervals.

Figure 1 B-E shows optical images of GONRs and rGONRs incubated with LiP and H_2O_2 in the presence and absence of VA after 0 and 96 hours. The higher degree of transparency of vial I (GONRs + LiP + H_2O_2 + VA, Figure 1 D) compared to vial II (same composition as vial I but lacking VA) indicates that the presence of VA increases/accelerates the degradation of GONRs. No color change was observed in vials III and IV (Figures 1 B and D), indicating that the presence of H_2O_2 and LiP is required for the degradation reaction. Additionally, since the treatment conditions were identical for all the experimental and control groups, the lack of color change observed in vials III and IV (Figure 1 B and D) illustrates that the color changes in vials I and II (Figures 1 B and D) were likely not due to dilution of the solutions. For rGONRs, the lack of noticeable color change observed in vials II, III, and IV (Figure 1 E) after 96 hours of incubation implies that the presence of VA is critical for the degradation of rGONRs. From the visual observation of the experimental and control groups (Figures 1 B-E), it can be concluded that degradation occurs in GONRs in the presence of all three components (LiP, VA and H_2O_2; vial I) or in the presence of LiP and H_2O_2 (vial II); whereas for rGONRs, degradation was observed only in the presence of all three components (LiP, VA, and H_2O_2; vial I; Figure 1 E).

TEM imaging was used to study the morphological changes in GONRs and rGONRs before and after LiP treatment. The length and width of the pristine GONRs (Figure 2 A) and rGONRs (Figure 2 E) were ~ 2 μm and 500-600 nm, respectively, confirming the complete unzipping of MWCNTs possessing diameters ranging from 110-170 nm (π * diameter). After 4 hours of incubation, the presence of numerous small diameter holes (13.5 ± 7.0 nm; Figure 2 B,

nanoribbon area marked with yellow circle) and wrinkles (Figure 2 B, black arrows) on the GONRs, and the nearly pristine structure of rGONRs (only a few small-diameter holes; Figure 2 F, black arrows), suggest that GONRs degrade at a faster rate than rGONRs. The structural degradation of rGONRs, marked by the presence of several small holes and cleavage of rGONR architecture, started after 72 hours (Figure 2 H, black arrows and Figure S1). The presence of amorphous carbonaceous aggregates (Figure 2 D) after 96 hours of incubation suggests complete structural degradation of GONRs. On the other hand, the presence of holes extending from the outer to inner layers of the rGONR sheets (Figure 2 H) suggests the formation of holey graphene, similar to the porous graphene produced by gold-nanoparticle-mediated hydroxyl radical attack on rGO [50].

Degradation of GONRs by LiP in the presence of H_2O_2 and absence of VA began after 48 hours, implying that the degradation process is accelerated in the presence of VA (degradation of GONRs began after 4 hours [Figure 2 B, black arrows] in the presence of VA). Furthermore, in the absence of VA, no structural degradation was observed in the rGONRs even after 96 hours of incubation (Figure S3 B), suggesting that LiP in the presence of H_2O_2 alone does not degrade rGONRs. The TEM analysis and Raman spectroscopy results taken together indicate that GONRs can be degraded by LiP in the presence of H_2O_2, and that the degradation process can be accelerated by the addition of VA. These results also imply that for the degradation of rGONRs, the presence of VA is critical. Furthermore, in the presence of VA, the degradation rate of GONRs and rGONRs by LiP is different. The delay in the formation of structural defects (holes) on rGONRs (after 48 hours) compared to GONRs (after 4 hours) provides further evidence that

the degradation kinetics is dependent on the substrate chemistry (oxidized vs. reduced graphene nanoribbon sheets).

Raman spectroscopy was performed to characterize the perturbations (chemical changes, structural defects) caused by the interaction of LiP and other cofactors (VA, H_2O_2) with nanoribbons. Raman peaks observed at 1370 cm^{-1} (D band) correspond to disorder in sp^2 hybridized carbon systems, and at 1600 cm^{-1} (G band) correspond to the in-plane stretching of carbon bonds [48]. The observed disappearance of the D and G bands (Figure 3 A and E) implies complete degradation of the graphene nanoribbon structure, suggesting the high efficiency of LiP (in the presence of VA and H_2O_2) in degrading GONRs. An increase in the I_D/I_G ratio corresponds to an increase in the number of defects (disruption of C=C bonds due to structural defects and/or presence of functional groups) in graphene [48, 51]. An initial increase in the I_D/I_G ratio was observed for the second vial (GONRs + LiP, Figure 3 B and F), which decreased at the end of the degradation process. An initial increase in the I_D/I_G ratio corresponds to the presence of defects on graphene, whereas the decrease in the I_D/I_G ratio at later time points may correspond to disintegration of the multiple stacked layers of graphene due to progressive degradation exposing the pristine graphene layers present beneath the outermost layer [32]. The Raman spectra from these pristine graphene layers would have an intense G band contribution, reducing the I_D/I_G ratio. A similar phenomenon (initial increase followed by progressive decrease in the I_D/I_G ratio) was observed during the enzymatic degradation of multiwalled carbon nanotubes, where HRP destroyed the outer layers, resulting in the exposure of pristine inner nanotube layers, thereby reducing the I_D/I_G ratio [37]. The GONRs and rGONRs used in this study were synthesized by the longitudinal unzipping of multiwalled carbon nanotubes, and

possess multiple stacked layers of graphene. In the absence of VA, LiP may be degrading the outer graphitic layers, thereby exposing the inner pristine layers leading to a decrease in the I_D/I_G ratio. These results strongly hint that the presence of VA accelerates the degradation phenomenon by forming structural defects that extend to the inner layers of GONRs. In comparison to GONRs treated with LiP in the presence of VA and H_2O_2, a gradual increase in the I_D/I_G ratio was observed for rGONRs, suggesting that the rate of degradation of rGONRs is slower compared to that of GONRs. In the absence of VA, no change in the I_D/I_G ratio was observed (Figure 3 D and H), indicating the lack of degradation of rGONRs. The results of the Raman spectroscopy suggest that LiP can degrade GONRs in either the presence or absence of VA (degradation is accelerated in the presence of VA); however, for the degradation of rGONRs, the presence of VA is critical.

LiP is a 38-46 kDa enzyme divided into N- and C- terminal domains with a heme structure inserted between the domains [44] (Figure 5 A). LiP forms compound I (Figure 5 B) through the oxidation of the enzyme by one molecule of hydrogen peroxide. Compound I is then reduced back to its original form via two reduction reactions leading to the formation of an intermediate -- compound II [40]. Excess H_2O_2 reacts with compound II forming a catalytic inactive form -- compound III. During the degradation reaction, VA serves multiple roles: (1) it is a good substrate for compound I and II and can protect the enzyme from forming the inactive compound III, thereby facilitating the regeneration of LiP [52]; and (2) it can act as a mediator in electron-transfer reactions forming $VA^{+\cdot}$ -, a cation radical that may oxidize substrates such as carbon nanomaterials, thereby reducing itself back to VA [53, 54]. This is especially important when the substrates are difficult to be oxidized [53], too slow to bind the enzyme [55], or too large in size

compared to the catalytic site [56] (such as GONRs and rGONRs). Thus, we hypothesize that the presence of VA facilitates the conversion of inactive compound III to active LiP [40], thereby accelerating the degradation of the substrates GONRs and rGONRs.

To the best of our knowledge, this is the first systematic study investigating the effects of LiP-induced degradation of oxidized and reduced graphene (GONRs and rGONRs). Other studies focused on the enzymatic degradation of carbon nanomaterials have employed two other peroxidase enzymes, namely (1) HRP, a widely used enzyme produced by the horseradish plant (*Armoracia rusticana*) [57] and (2) human MPO, an enzyme found in the human immune system [58]. Kotchey et al. reported on the degradation of graphene oxide (formation of holes in the basal place) using HRP in the presence of low concentrations of H_2O_2 (~ 40 μM) [32], and Russier et al. compared the degradation of oxidized SWCNTs and MWCNTs by HRP [28]. In their study, after 60 days, complete degradation of oxidized SWCNTs and partial degradation of oxidized MWCNTs were observed. Kagan et al. reported the degradation of oxidized SWCNTs using MPO [35]. They found that, after 12 hours of incubation of oxidized SWCNTs with MPO and H_2O_2, the presence of short short-chain carboxylated alkanes and alkenes was observed in the degradation products. Importantly, however, the aforementioned studies reported enzymatic degradation of oxidized carbon nanomaterials; pristine or chemically reduced carbon nanomaterials could not be degraded by HRP and MPO.

We have previously reported that pristine graphene sheets synthesized by chemical vapor deposition could also degrade at H_2O_2 concentrations present in the environment without the

need of peroxidase enzymes, albeit at a slower degradation rate [30]. Lignin peroxidase, produced by fungal species such as *Phanerochaete chrysosporium* [40], possesses higher redox potential (up to 1.4 V) [41] compared to HRP (0.941-0.96 V) [42] and MPO (0.97-1.35V) [43], suggesting that between LiP, MPO, and HRP; LiP has a stronger potential to oxidize substrates. Therefore, the effects of LiP-induced structural degradation on oxidized and reduced graphene (GONRs and rGONRs) were systematically investigated in this study. Our results show that LiP, in the presence of VA and H_2O_2, can degrade GONRs and rGONRs at substantially lower degradation times; GONRs required only 96 hours.

Several studies have highlighted the uncertain long-term environmental and physiological effects of carbon nanomaterials [8, 23-27]. The ubiquitous presence of white rot fungi, and thus LiP, in the environment suggests that this organism could eventually degrade graphene nanoparticles released into the environment. This fungus grows by hyphal extension through the soil, and has an advantage in gaining better excess to pollutants accumulated in soil pores [59]. However, pollutants broken down by white rot fungi are typically present in small amounts (part per million levels). Thus, macroscopic amounts of graphene will degrade slowly in the environment. Nevertheless, white rot fungi are attractive candidates for environmental remediation of graphene for several reasons [59-63]: (1) they can be present in more concentrated amounts, and thus, be employed to more efficiently degrade graphene. (2) They can be easily isolated and used for remediation purposes. (3) In addition to LiP, white rot fungi release a multitude of enzymes (such as laccase, manganese peroxidase, etc.) responsible for biodegradation of complex organic compounds. These enzymes are expressed under nitrogen starvation, and therefore, the fungi do not have to be acclimatized for graphene degradation. (4) The LiP degradation system is

extracellular and non-specific, thereby eliminating the need for pre-oxidation of graphene, unlike the HRP and MPO degradation systems, which require treatment with strong acids before enzymatic degradation. Additionally, the extracellular degradation mechanism eliminates the need for graphene internalization by fungal hyphae. (5) Lastly, white rot fungi use relatively cheap sources of carbon such as sawdust, corncobs, straws etc., which can be readily provided for easy colonization and biomass production.

Conclusions:

GONRs and rGONRs interact with LiP; a ligninolytic enzyme released from white rot fungus in the presence and absence of VA. Within 96 hours, in the presence of H_2O_2 and VA, GONRs and rGONRs were completely and partially degraded by LiP, respectively. The structural degradation of GONRs and rGONRs commenced after 4 and 48 hours of incubation with LiP, VA, and H_2O_2, respectively. The delay in the degradation of rGONRs suggests that the degradation kinetics is dependent on the substrate chemistry (oxidized vs. reduced nanoribbons). In the absence of VA, no structural degradation of rGONRs was observed at all time points, suggesting that VA may be a critical factor for the degradation of rGONRs. The results indicate that LiP (possessing higher theoretical redox potential than MPO or HRP) can efficiently degrade GONRs and rGONRs in the presence of VA. The ubiquitous presence of white rot fungi, and thus LiP, in the environment suggests that this organism could eventually degrade graphene nanoparticles released into the environment.

Acknowledgements:

This work was supported by the National Institutes of Health (Grant No. 1DP2OD007394-01). The authors thank Susan Van Horn (Central Microscopy, Stony Brook University) for her help with TEM image acquisition and Ms. Cecelia Petrus for editorial help.

References

[1] Boehm H-P. Graphene—How a Laboratory Curiosity Suddenly Became Extremely Interesting. Angewandte Chemie International Edition. 2010;49:9332-5.

[2] Boehm HP, Setton R, Stumpp E. Nomenclature and terminology of graphite intercalation compounds. Carbon. 1986;24:241-5.

[3] Geim AK, Novoselov KS. The rise of graphene. Nature materials. 2007;6:183-91.

[4] Li X, Wang X, Zhang L, Lee S, Dai H. Chemically derived, ultrasmooth graphene nanoribbon semiconductors. Science. 2008;319:1229-32.

[5] Ritter Ka Fau - Lyding JW, Lyding JW. The influence of edge structure on the electronic properties of graphene quantum dots and nanoribbons. Natural Materials. 2009;8.

[6] Kauffman DR, Star A. Graphene versus carbon nanotubes for chemical sensor and fuel cell applications. The Analyst. 2010;135:2790-7.

[7] Mullick Chowdhury S, Lalwani G, Zhang K, Yang JY, Neville K, Sitharaman B. Cell specific cytotoxicity and uptake of graphene nanoribbons. Biomaterials. 2013;34:283-93.

[8] Feng L, Liu Z. Graphene in biomedicine: opportunities and challenges. Nanomedicine. 2011;6:317-24.

[9] Kanakia S, Toussaint JD, Chowdhury SM, Lalwani G, Tembulkar T, Button T, et al. Physicochemical characterization of a novel graphene-based magnetic resonance imaging contrast agent. International journal of nanomedicine. 2013;8:2821-33.

[10] Lalwani G, Cai X, Nie L, Wang LV, Sitharaman B. Graphene-based contrast agents for photoacoustic and thermoacoustic tomography. Photoacoustics. 2013;1:62-7.

[11] Yang K, Zhang S, Zhang G, Sun X, Lee ST, Liu Z. Graphene in mice: ultrahigh in vivo tumor uptake and efficient photothermal therapy. Nano letters. 2010;10:3318-23.

[12] Tian B, Wang C, Zhang S, Feng L, Liu Z. Photothermally enhanced photodynamic therapy delivered by nano-graphene oxide. ACS nano. 2011;5:7000-9.

[13] Lalwani G, Kwaczala AT, Kanakia S, Patel SC, Judex S, Sitharaman B. Fabrication and Characterization of Three-Dimensional Macroscopic All-Carbon Scaffolds. Carbon N Y. 2013;53:90-100.

[14] Lalwani G, Henslee AM, Farshid B, Lin L, Kasper FK, Qin YX, et al. Two-dimensional nanostructure-reinforced biodegradable polymeric nanocomposites for bone tissue engineering. Biomacromolecules. 2013;14:900-9.

[15] Zhou M, Zhai Y, Dong S. Electrochemical sensing and biosensing platform based on chemically reduced graphene oxide. Analytical chemistry. 2009;81:5603-13.

[16] Robinson JT, Perkins FK, Snow ES, Wei Z, Sheehan PE. Reduced graphene oxide molecular sensors. Nano letters. 2008;8:3137-40.

[17] Talukdar Y, Rashkow J, Lalwani G, Kanakia S, Sitharaman B. The Effect of Graphene Nanostructures on Mesenchymal Stem Cells. Biomaterials. 2014;35:4863–77.

[18] Lalwani G, Sundararaj JL, Schaefer K, Button T, Sitharaman B. Synthesis, Characterization, In Vitro Phantom Imaging, and Cytotoxicity of A Novel Graphene-Based Multimodal Magnetic Resonance Imaging - X-Ray Computed Tomography Contrast Agent. Journal of Materials Chemistry B. 2014;2:3519-30.

[19] Zhu Y, Murali S, Cai W, Li X, Suk JW, Potts JR, et al. Graphene and graphene oxide: synthesis, properties, and applications. Advanced materials. 2010;22:3906-24.

[20] Pei S, Cheng H-M. The reduction of graphene oxide. Carbon. 2012;50:3210-28.

[21] Zhang X, Yin J, Peng C, Hu W, Zhu Z, Li W, et al. Distribution and biocompatibility studies of graphene oxide in mice after intravenous administration. Carbon. 2011;49:986-95.

[22] Liu Y, Yu D, Zeng C, Miao Z, Dai L. Biocompatible Graphene Oxide-Based Glucose Biosensors. Langmuir. 2010;26:6158-60.

[23] Chang Y, Yang ST, Liu JH, Dong E, Wang Y, Cao A, et al. In vitro toxicity evaluation of graphene oxide on A549 cells. Toxicology letters. 2011;200:201-10.

[24] Wang K, Ruan J, Song H, Zhang J, Wo Y, Guo S, et al. Biocompatibility of Graphene Oxide. Nanoscale Research Letters. 2010.

[25] Klaine SJ, Alvarez PJ, Batley GE, Fernandes TF, Handy RD, Lyon DY, et al. Nanomaterials in the environment: behavior, fate, bioavailability, and effects. Environmental toxicology and chemistry / SETAC. 2008;27:1825-51.

[26] Lalwani G, Sitharaman B. Multifunctional Fullerene- and Metallofullerene-Based Nanobiomaterials. Nano LIFE. 2013;03:1342003.

[27] Petersen EJ, Zhang L, Mattison NT, O'Carroll DM, Whelton AJ, Uddin N, et al. Potential release pathways, environmental fate, and ecological risks of carbon nanotubes. Environmental science & technology. 2011;45:9837-56.

[28] Russier J, Menard-Moyon C, Venturelli E, Gravel E, Marcolongo G, Meneghetti M, et al. Oxidative biodegradation of single- and multi-walled carbon nanotubes. Nanoscale. 2011;3:893-6.

[29] Vlasova II, Vakhrusheva TV, Sokolov AV, Kostevich VA, Ragimov AA. Peroxidase-induced degradation of single-walled carbon nanotubes: hypochlorite is a major oxidant capable ofin vivodegradation of carbon nanotubes. Journal of Physics: Conference Series. 2011;291:012056.

[30] Xing W, Lalwani G, Rusakova I, Sitharaman B. Degradation of Graphene by Hydrogen Peroxide. Particle & Particle Systems Characterization. 2014;31:745-50.

[31] Peng Y, Liu H. Effects of Oxidation by Hydrogen Peroxide on the Structures of Multiwalled Carbon Nanotubes. Industrial & Engineering Chemistry Research. 2006;45:6483-8.

[32] Kotchey GP, Allen BL, Vedala H, Yanamala N, Kapralov AA, Tyurina YY, et al. The enzymatic oxidation of graphene oxide. ACS nano. 2011;5:2098-108.

[33] Allen BL, Kichambare PD, Gou P, Vlasova, II, Kapralov AA, Konduru N, et al. Biodegradation of single-walled carbon nanotubes through enzymatic catalysis. Nano letters. 2008;8:3899-903.

[34] Allen BL, Kotchey GP, Chen Y, Yanamala NV, Klein-Seetharaman J, Kagan VE, et al. Mechanistic investigations of horseradish peroxidase-catalyzed degradation of single-walled carbon nanotubes. Journal of the American Chemical Society. 2009;131:17194-205.

[35] Kagan VE, Konduru NV, Feng W, Allen BL, Conroy J, Volkov Y, et al. Carbon nanotubes degraded by neutrophil myeloperoxidase induce less pulmonary inflammation. Nature nanotechnology. 2010;5:354-9.

[36] Kotchey GP, Hasan SA, Kapralov AA, Ha SH, Kim K, Shvedova AA, et al. A natural vanishing act: the enzyme-catalyzed degradation of carbon nanomaterials. Accounts of chemical research. 2012;45:1770-81.

[37] Zhao Y, Allen BL, Star A. Enzymatic degradation of multiwalled carbon nanotubes. The journal of physical chemistry A. 2011;115:9536-44.

[38] Leatham GF. The ligninolytic activities of Lentinus edodes and Phanerochaete chrysosporium. Applied microbiology and biotechnology. 1986;24:51-8.

[39] Tien M, Kirk TK. Lignin-degrading enzyme from the hymenomycete Phanerochaete chrysosporium Burds. Science(Washington). 1983;221:661-2.

[40] Ten Have R, Teunissen PJ. Oxidative mechanisms involved in lignin degradation by white-rot fungi. Chemical reviews. 2001;101:3397-413.

[41] Valli K, Wariishi H, Gold MH. Oxidation of monomethoxylated aromatic compounds by lignin peroxidase: role of veratryl alcohol in lignin biodegradation. Biochemistry. 1990;29:8535-9.

[42] Hayashi Y, Yamazaki I. The oxidation-reduction potentials of compound I/compound II and compound II/ferric couples of horseradish peroxidases A2 and C. The Journal of biological chemistry. 1979;254:9101-6.

[43] Arnhold J. Properties, functions, and secretion of human myeloperoxidase. Biochemistry Biokhimiia. 2004;69:4-9.

[44] Wong DW. Structure and action mechanism of ligninolytic enzymes. Applied biochemistry and biotechnology. 2009;157:174-209.

[45] Kosynkin DV, Higginbotham AL, Sinitskii A, Lomeda JR, Dimiev A, Price BK, et al. Longitudinal unzipping of carbon nanotubes to form graphene nanoribbons. Nature. 2009;458:872-6.

[46] Higginbotham AL, Kosynkin DV, Sinitskii A, Sun Z, Tour JM. Lower-defect graphene oxide nanoribbons from multiwalled carbon nanotubes. ACS nano. 2010;4:2059-69.

[47] Linko S, Haapala R. A critical study of lignin peroxidase activity assay by veratryl alcohol oxidation. Biotechnol Tech. 1993;7:75-80.

[48] Dresselhaus MS, Jorio A, Hofmann M, Dresselhaus G, Saito R. Perspectives on carbon nanotubes and graphene Raman spectroscopy. Nano letters. 2010;10:751-8.

[49] Tien M, Kirk TK. Lignin peroxidase of Phanerochaete chrysosporium. In: Willis A. Wood STK, editor. Methods in Enzymology: Academic Press; 1988. p. 238-49.

[50] Radich JG, Kamat PV. Making graphene holey. Gold-nanoparticle-mediated hydroxyl radical attack on reduced graphene oxide. ACS nano. 2013;7:5546-57.

[51] Ouyang Y, Cong LM, Chen L, Liu QX, Fang Y. Raman study on single-walled carbon nanotubes and multi-walled carbon nanotubes with different laser excitation energies. Physica E: Low-dimensional Systems and Nanostructures. 2008;40:2386-9.

[52] Cancel AM, Orth AB, Tien M. Lignin and veratryl alcohol are not inducers of the ligninolytic system of Phanerochaete chrysosporium. Applied and environmental microbiology. 1993;59:2909-13.

[53] Tien M, Ma D. Oxidation of 4-methoxymandelic acid by lignin peroxidase. Mediation by veratryl alcohol. The Journal of biological chemistry. 1997;272:8912-7.

[54] Goodwin DC, Aust SD, Grover TA. Evidence for veratryl alcohol as a redox mediator in lignin peroxidase-catalyzed oxidation. Biochemistry. 1995;34:5060-5.

[55] Akamatsu Y, Ma DB, Higuchi T, Shimada M. A novel enzymatic decarboxylation of oxalic acid by the lignin peroxidase system of white-rot fungus Phanerochaete chrysosporium. FEBS letters. 1990;269:261-3.

[56] Teunissen PJ, Field JA. 2-Chloro-1,4-dimethoxybenzene as a mediator of lignin peroxidase catalyzed oxidations. FEBS letters. 1998;439:219-23.

[57] Veitch NC. Horseradish peroxidase: a modern view of a classic enzyme. Phytochemistry. 2004;65:249-59.

[58] Hansson M, Olsson I, Nauseef WM. Biosynthesis, processing, and sorting of human myeloperoxidase. Archives of biochemistry and biophysics. 2006;445:214-24.

[59] Baldrian P. Wood-inhabiting ligninolytic basidiomycetes in soils: ecology and constraints for applicability in bioremediation. Fungal Ecology. 2008;1:4-12.

[60] Pointing S. Feasibility of bioremediation by white-rot fungi. Applied Microbiology and Biotechnology. 2001;57:20-33.

[61] Reddy CA, Mathew Z. Bioremediation potential of white rot fungi. British Mycological Society Symposium Series. 2001. p. 52-78.

[62] Shah MM, Barr DP, Chung N, Aust SD. Use of white rot fungi in the degradation of environmental chemicals. Toxicology letters. 1992;64-65 Spec No:493-501.

[63] Marco-Urrea E, Reddy C. Degradation of chloro-organic pollutants by white rot fungi. Microbial degradation of xenobiotics: Springer; 2012. p. 31-66.

Figure Legends:

Figure 1: (A) Enzyme kinetics of lignin peroxidase (LiP) with/without oxidized graphene oxide nanoribbons (GONRs) in the presence of veratryl alcohol (VA; substrate) to measure the consumption of hydrogen peroxide (H_2O_2). (B-E) Optical images of experimental and control group vials: (B and D) GONRs and (C and E) reduced graphene oxide nanoribbons (rGONRs) treated with/without LiP, VA, and H_2O_2 after 0 and 96 hours.

Figure 2: Representative transmission electron microscopy images of oxidized and reduced graphene oxide nanoribbons (GONRs and rGONRs). (A-D) GONRs and (E-H) rGONRs treated with lignin peroxidase, veratryl alcohol, and hydrogen peroxide after 0, 4, 48, and 96 hours. Arrows in (B, D and G) point to representative holes on the graphene sheets.

Figure 3: Representative Raman spectra of (A) oxidized graphene oxide nanoribbons (GONRs) treated with lignin peroxidase (LiP), veratryl alcohol (VA), and hydrogen peroxide (H_2O_2); (B) GONRs treated with LiP and H_2O_2; (C) reduced graphene oxide nanoribbons (rGONRs) treated

with LiP, VA, and H_2O_2; and (D) rGONRs treated with LiP and H_2O_2 after 0, 24, 72, and 96 hours. (E-H) Corresponding I_D/I_G intensity ratios for (A-D) at every time point.

Figure 4: Distribution plot of the hole diameter ('D') and distance between holes ('d') (see inset for description) of (A and B) oxidized graphene oxide nanoribbons (GONRs) after 4 and 96 hours, and (C and D) reduced graphene oxide nanoribbons (rGONRs) after 48 and 96 hours of incubation with lignin peroxidase, veratryl alcohol, and hydrogen peroxide.

Figure 5: (A) Lignin peroxidase (LiP) enzymatic cycle. (B) Ribbon diagram of LiP obtained from the Protein Data Bank (accession code 1B85). (C) Schematic representing the structural degradation of graphene nanoribbons.

Tables

Table 1: I_D/I_G ratio values for oxidized and reduced graphene oxide nanoribbons (GONRs and rGONRs) treated with lignin peroxidase in the presence/absence of veratryl alcohol (VA) after 0, 24, 72, and 96 hours.

Samples	Time points (hours)			
	0	24	72	96
GONRs with VA	1.32	1.38	1.76	1.89
GONRs without VA	1.32	1.41	1.64	1.49
rGONRs with VA	1.51	1.66	1.75	1.77
rGONRs without VA	1.51	1.81	1.64	1.70

Figure 1 A:

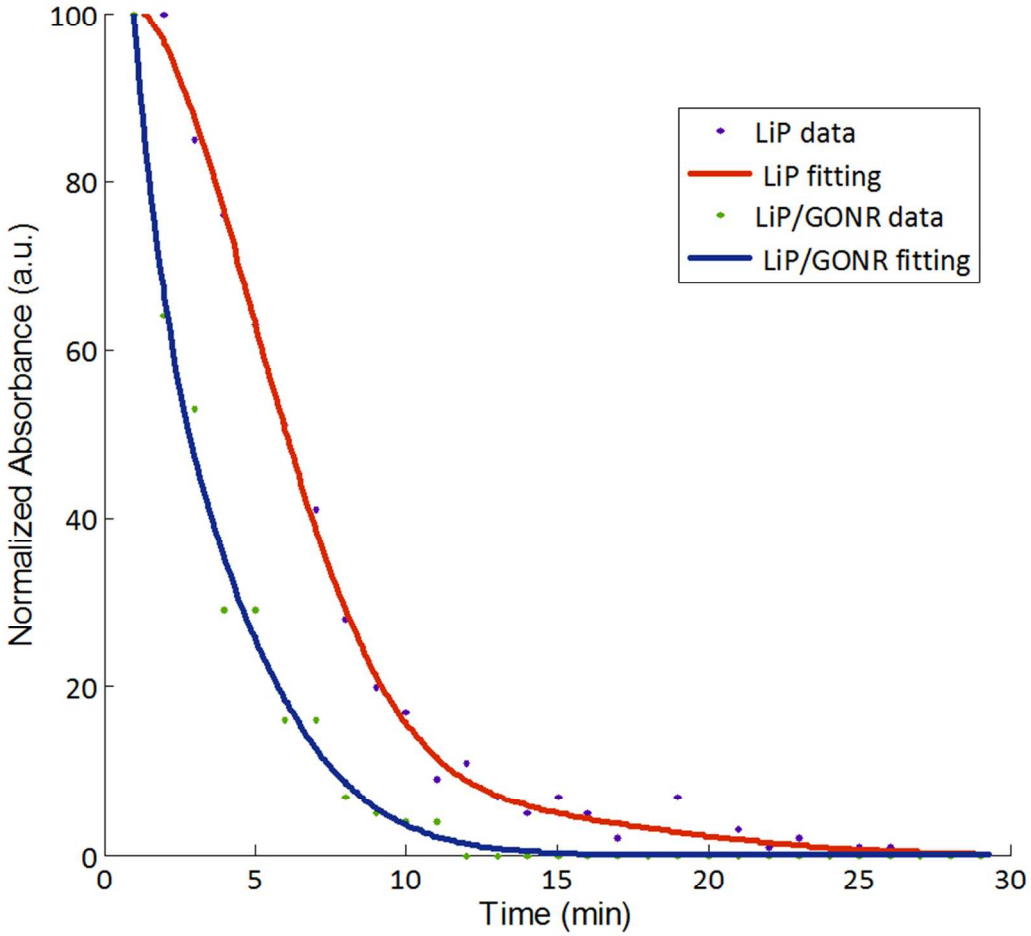

Figure 1 B-E:

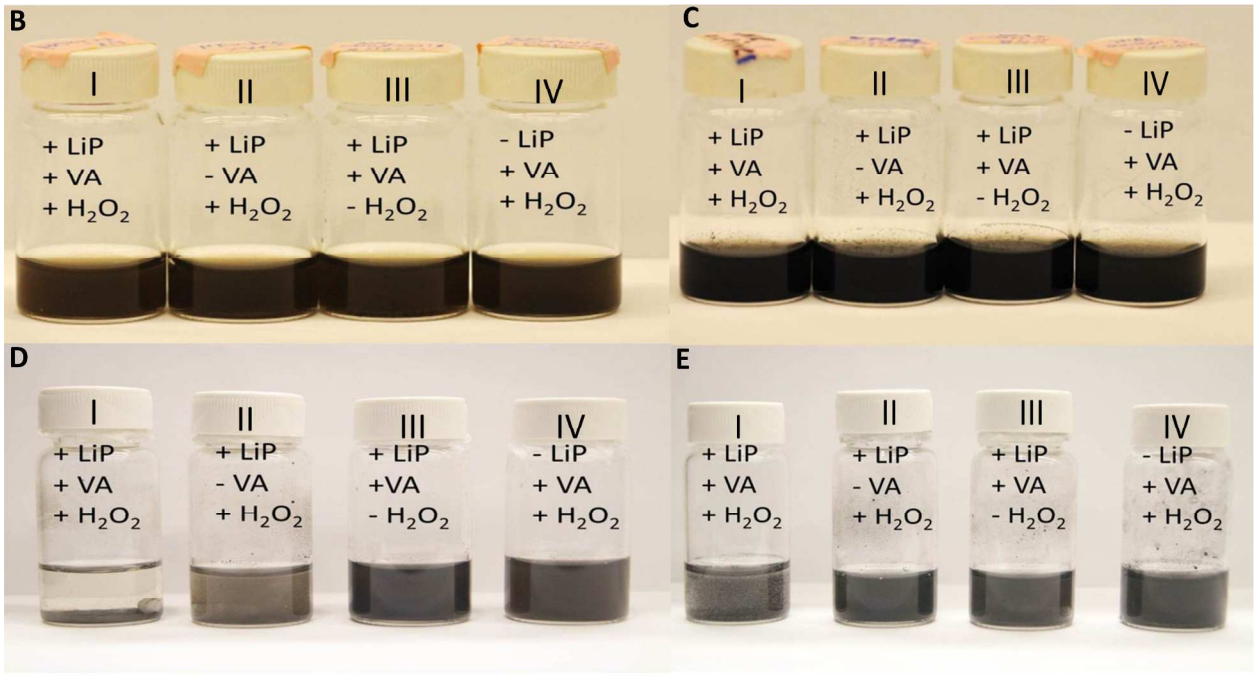

Figure 2 A:

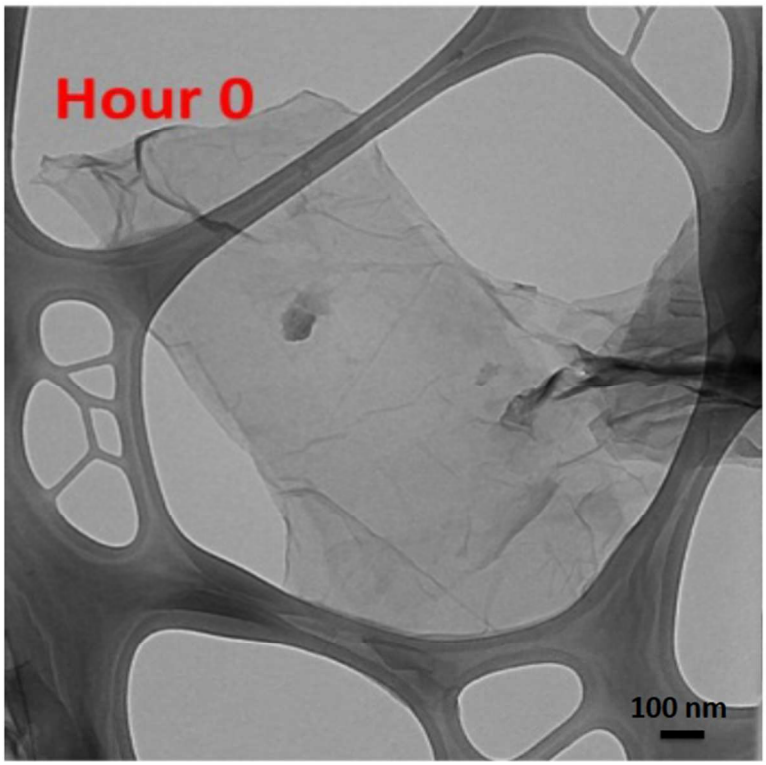

Figure 2 B:

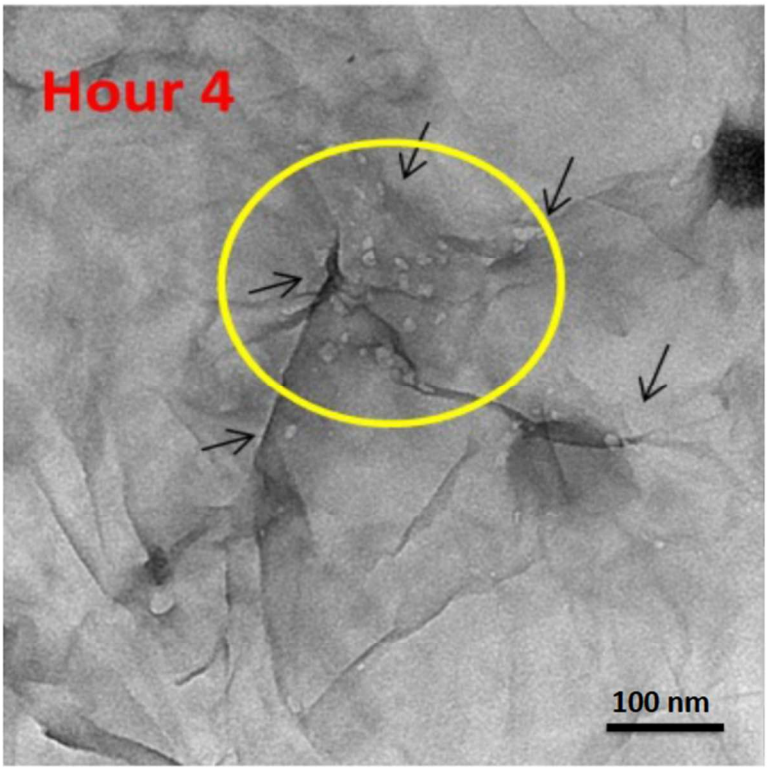

Figure 2 C:

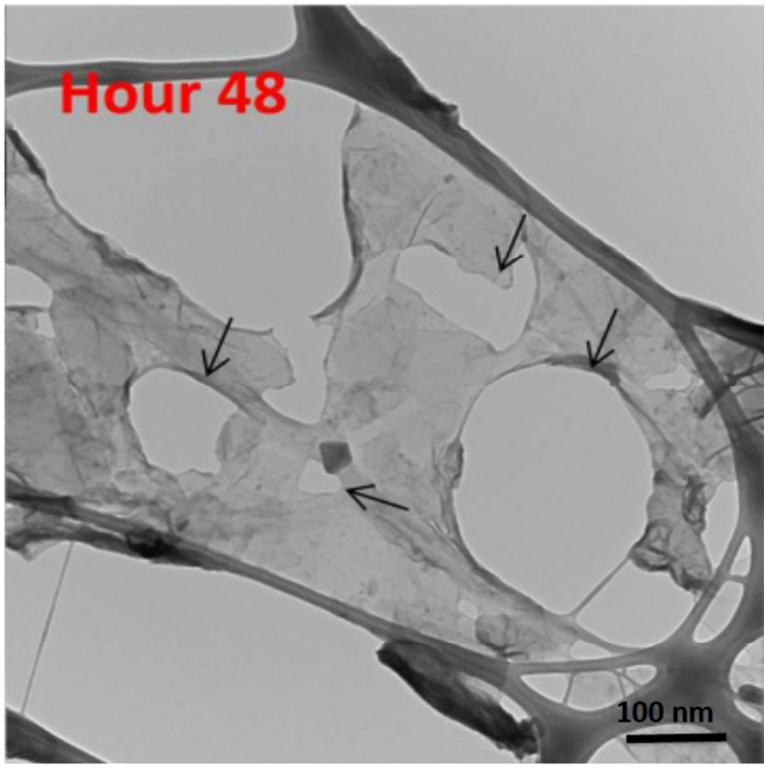

Figure 2 D:

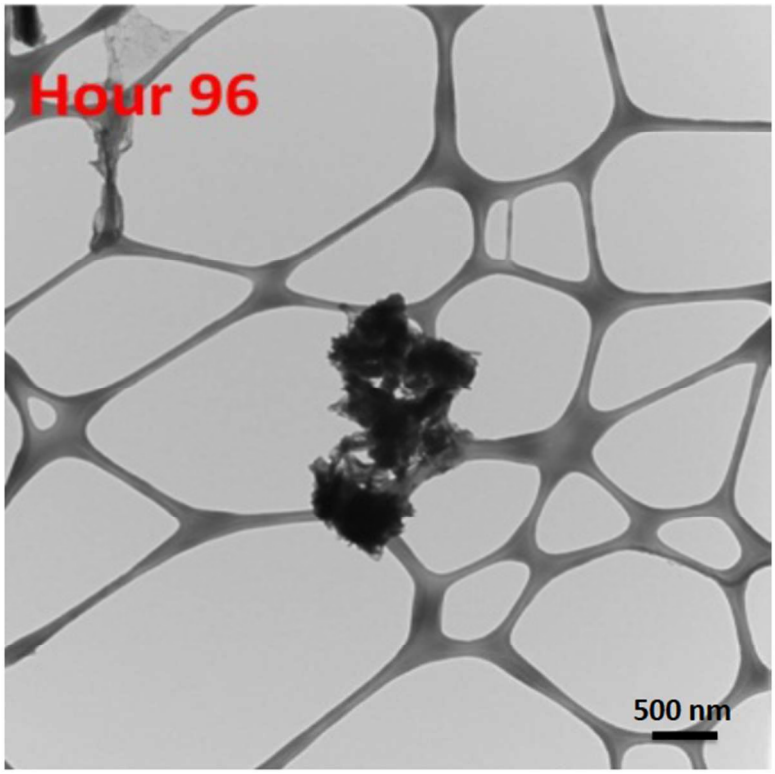

Figure 2 E:

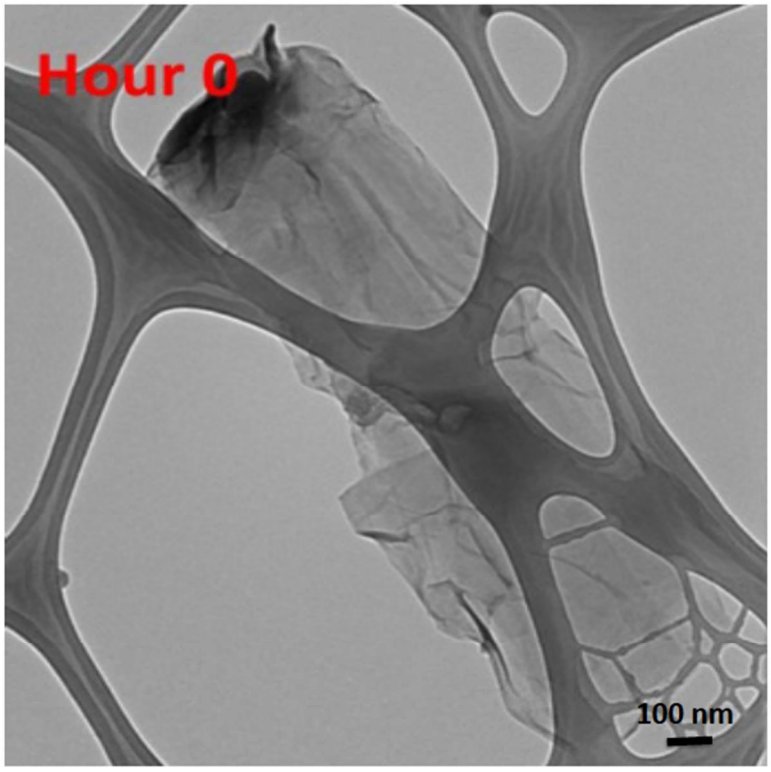

Figure 2 F:

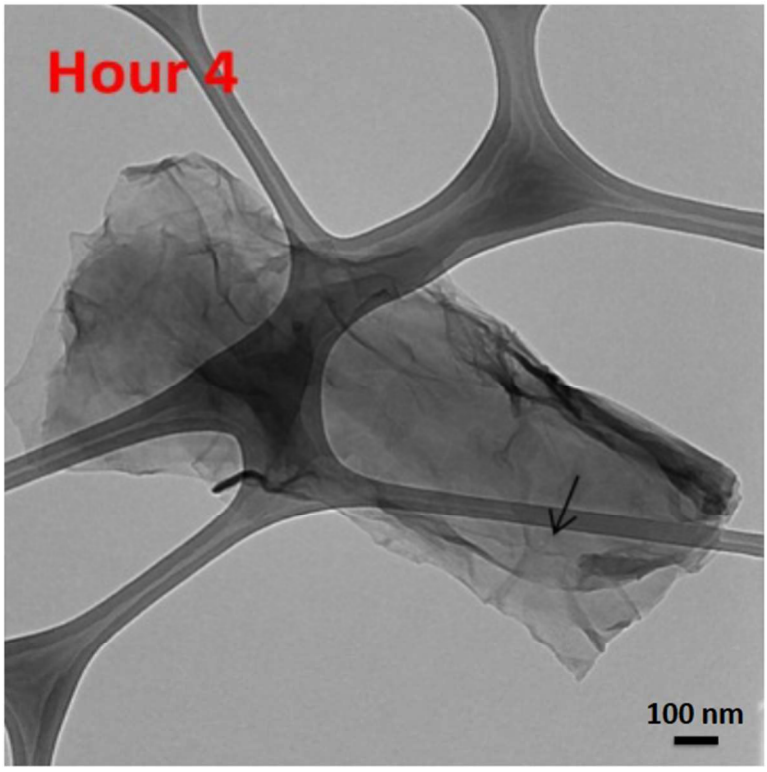

Figure 2 G:

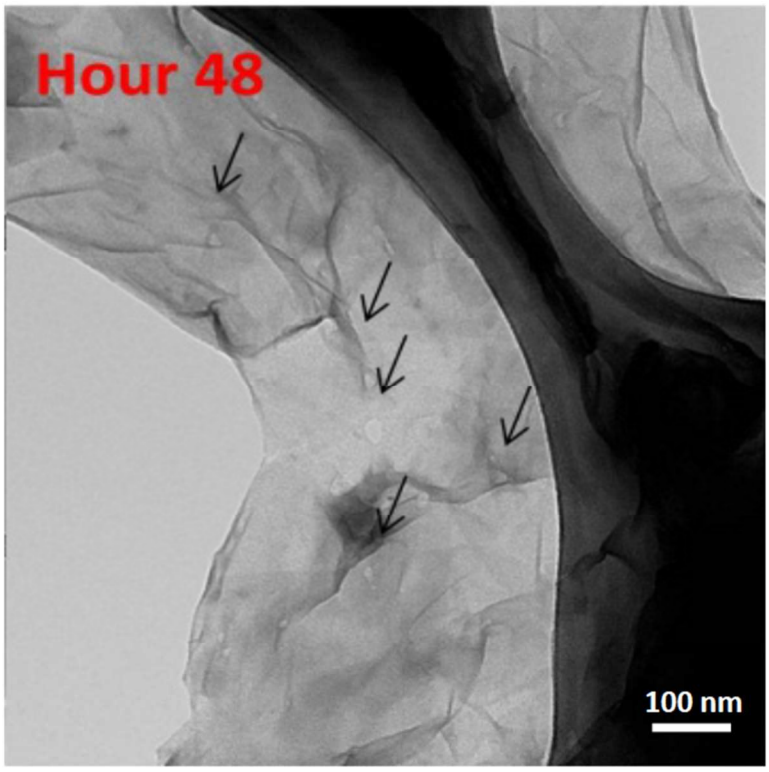

Figure 2 H:

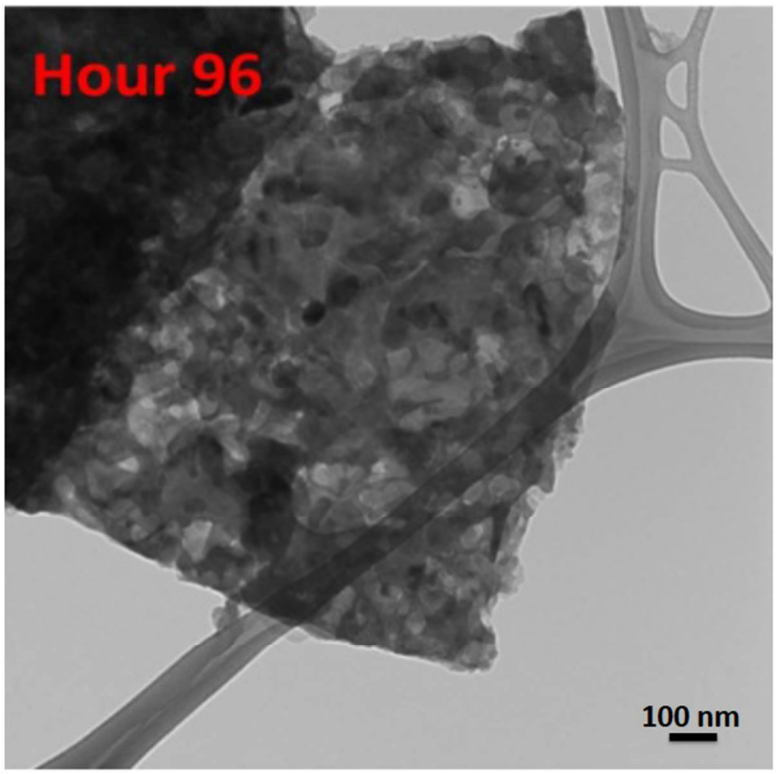

Figure 3 A:

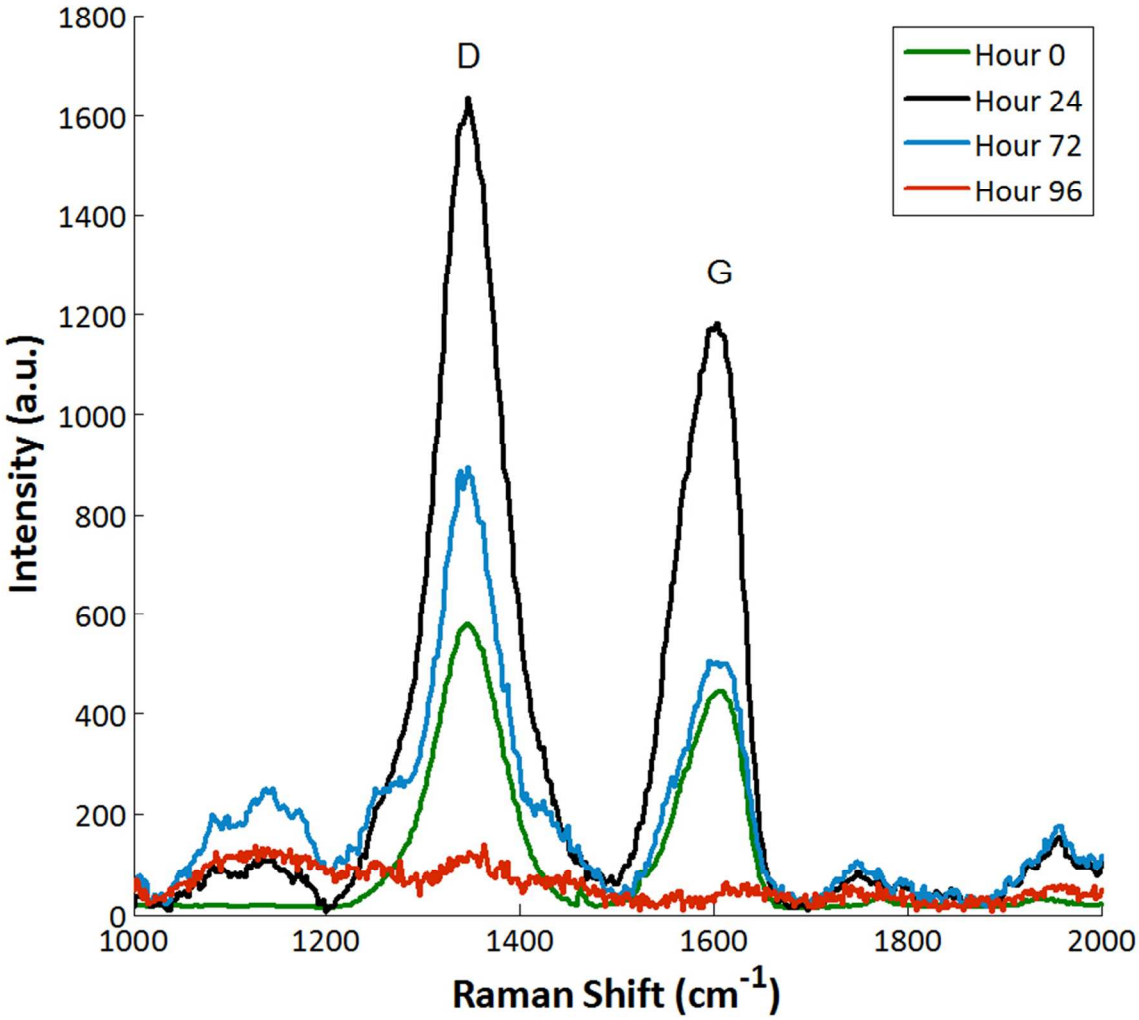

Figure 3 B:

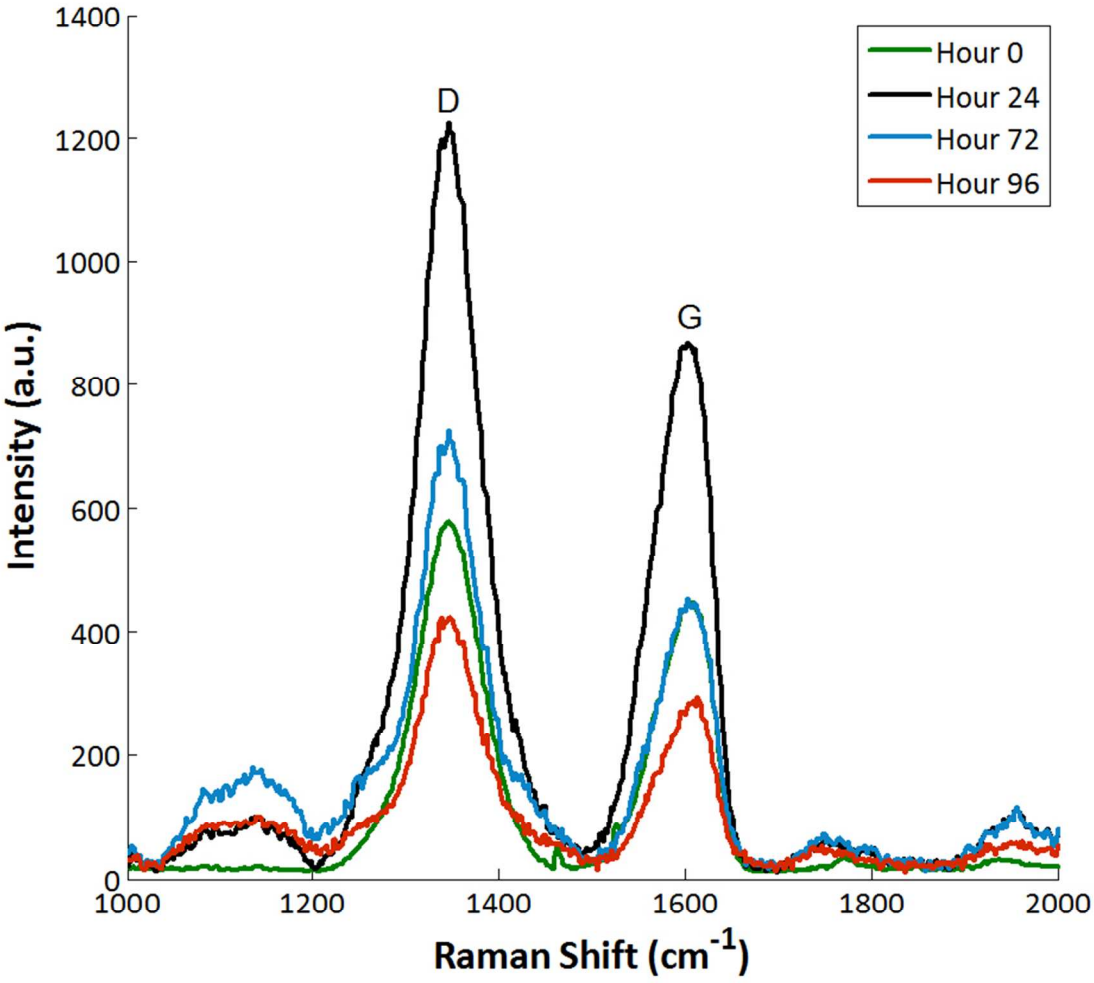

Figure 3 C:

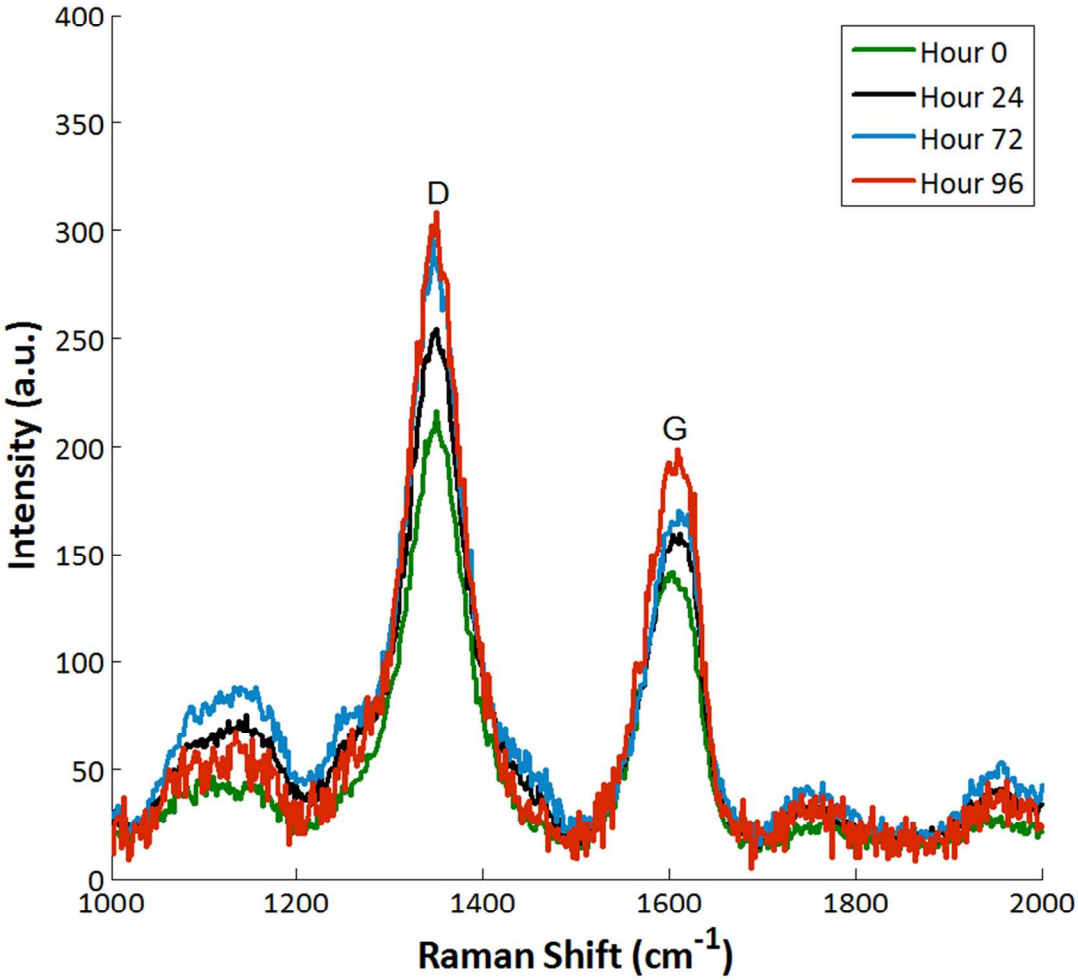

Figure 3 D:

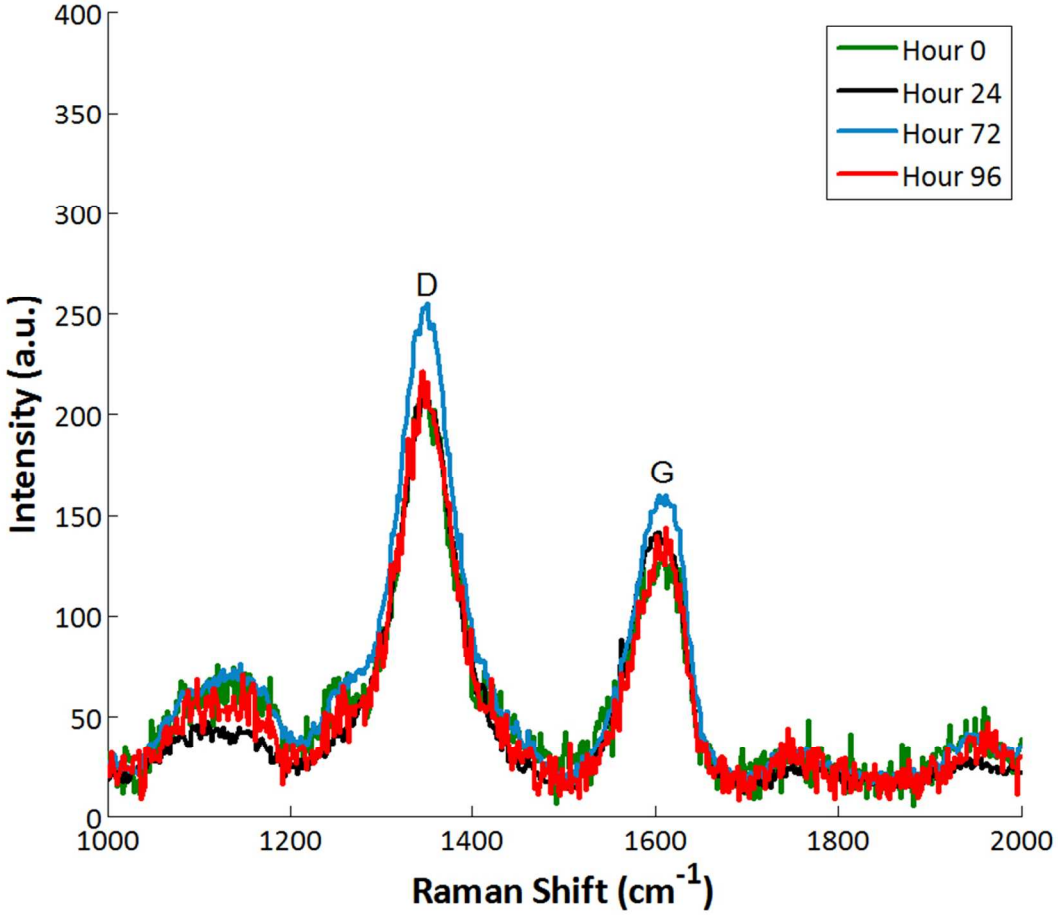

Figure 3 E:

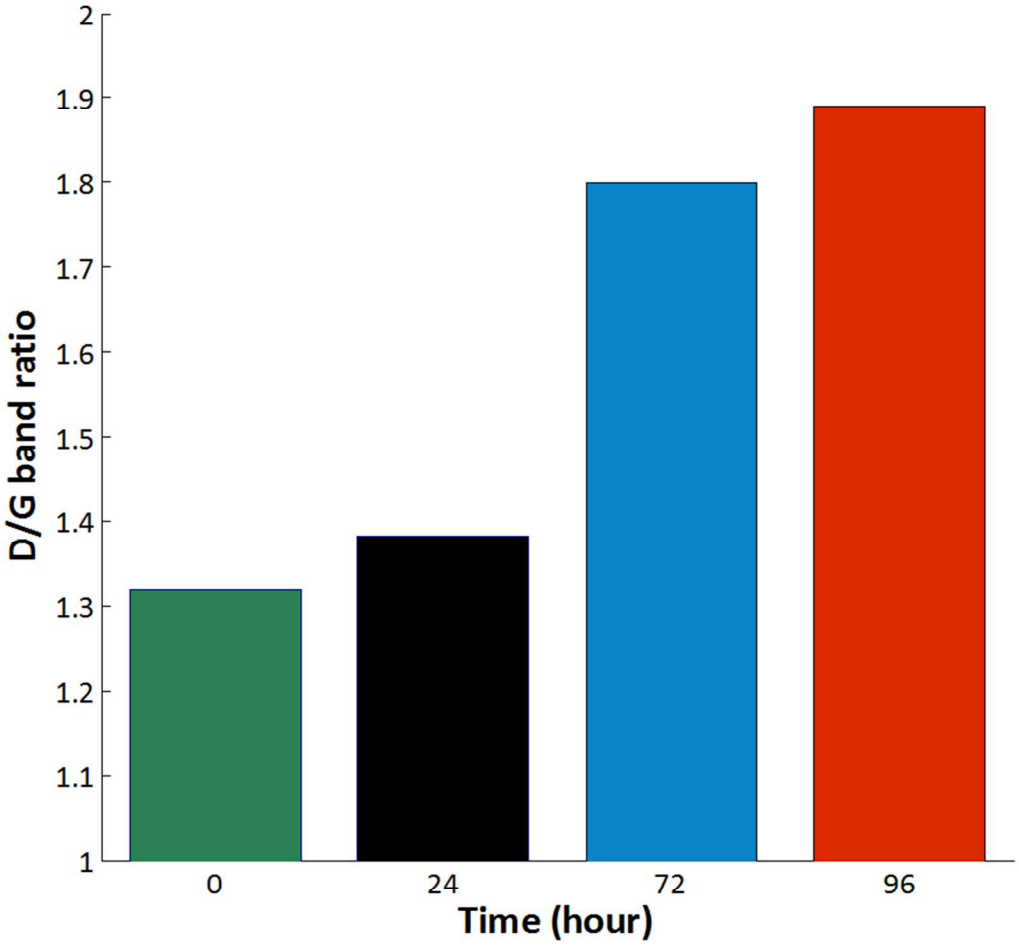

Figure 3 F:

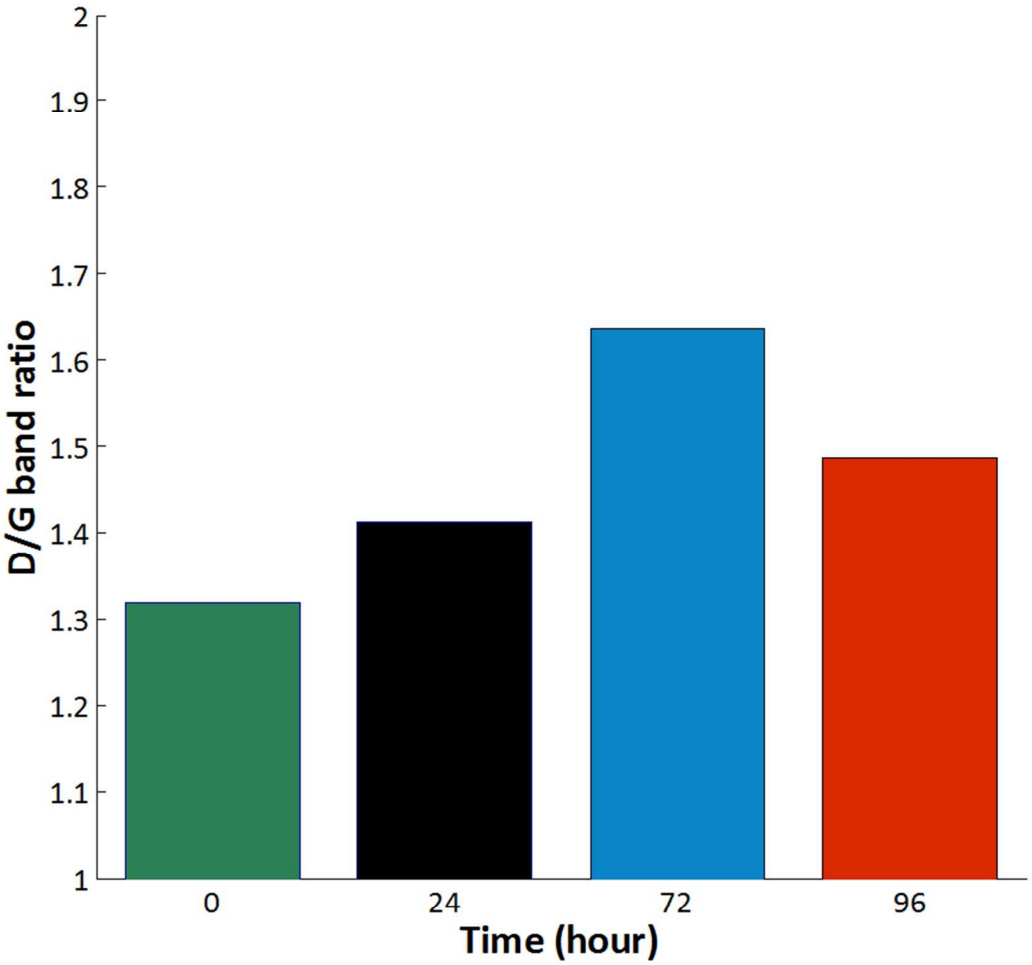

Figure 3 G:

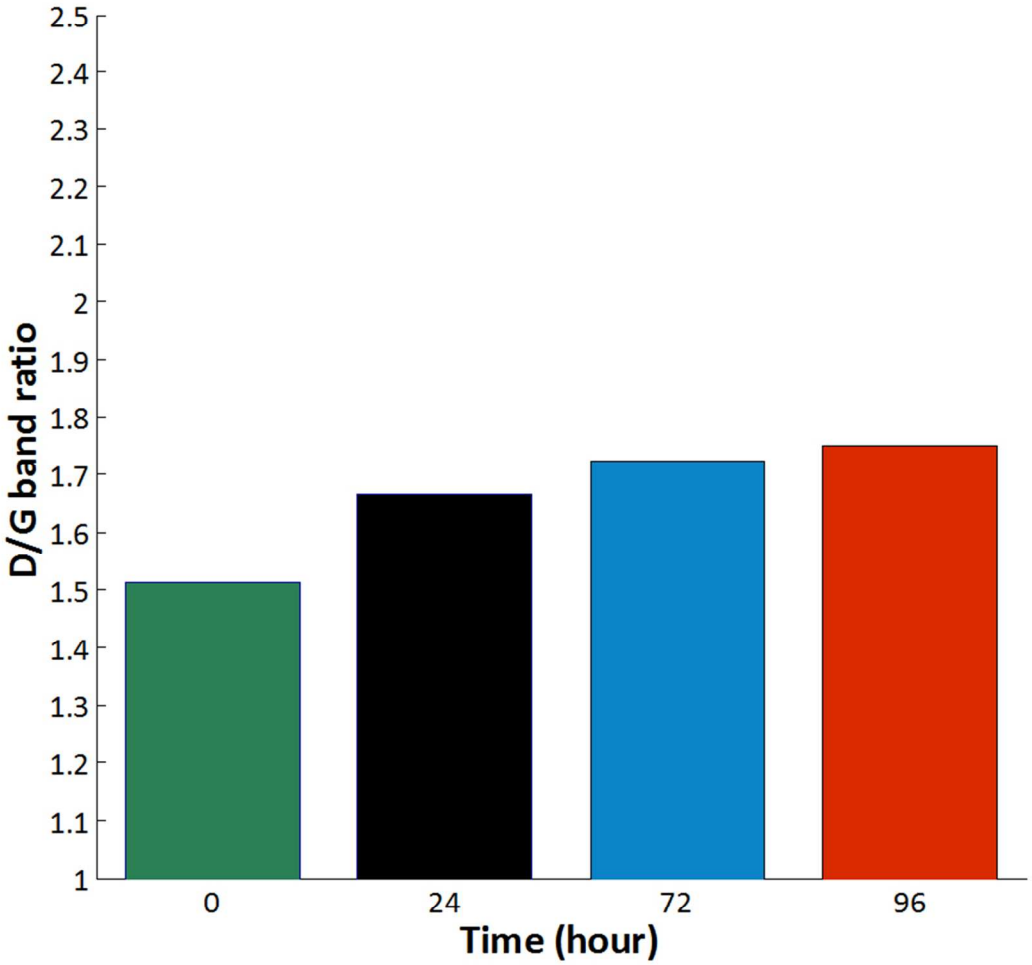

Figure 3 H:

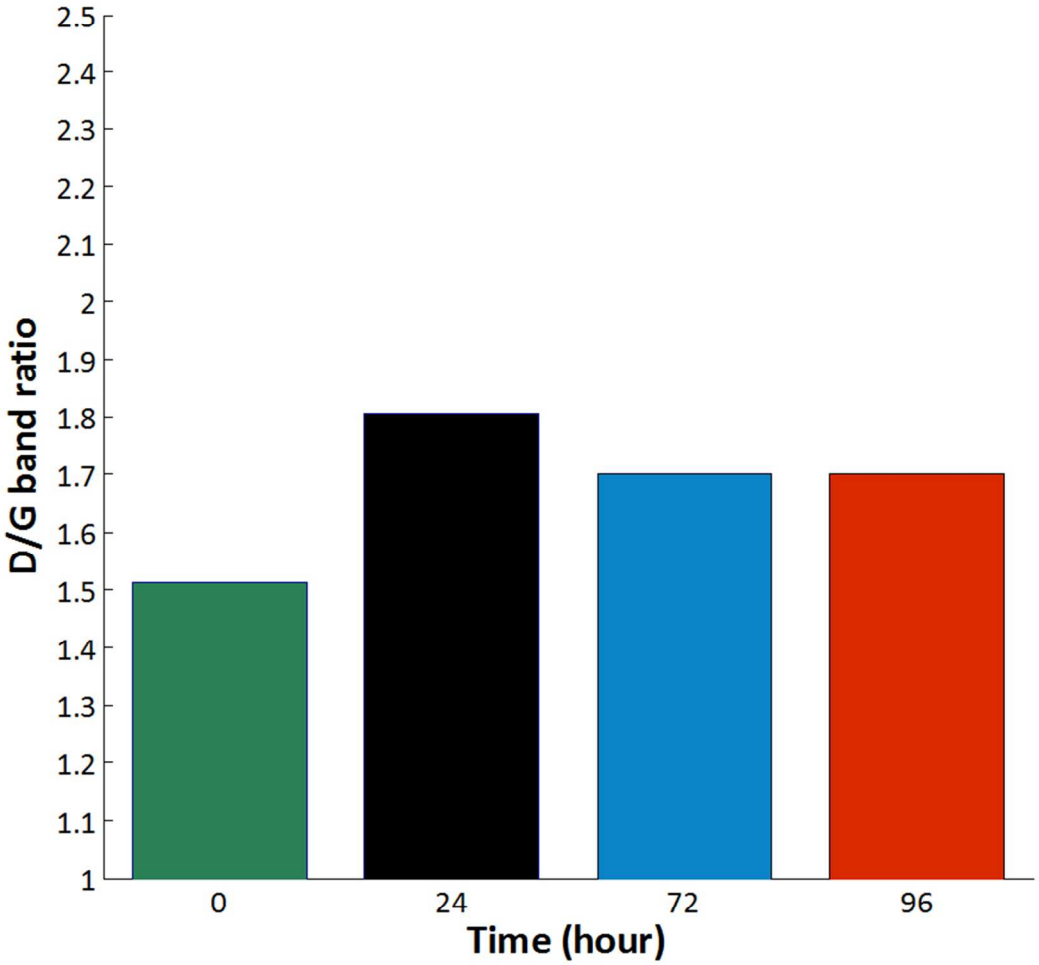

Figure 4 A:

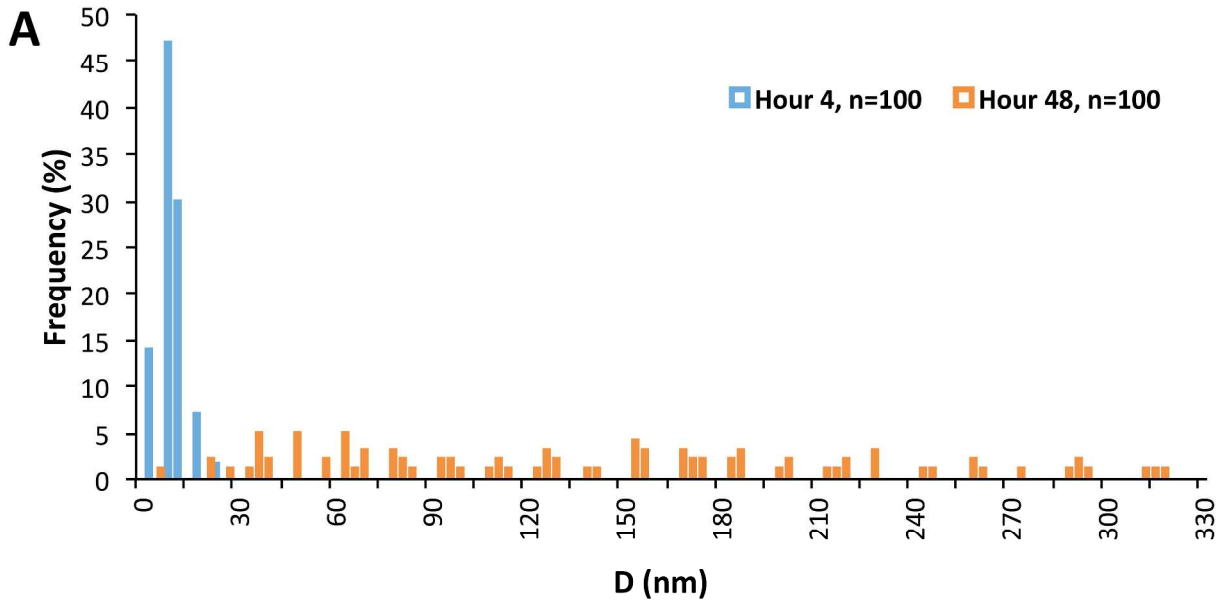

Figure 4 B:

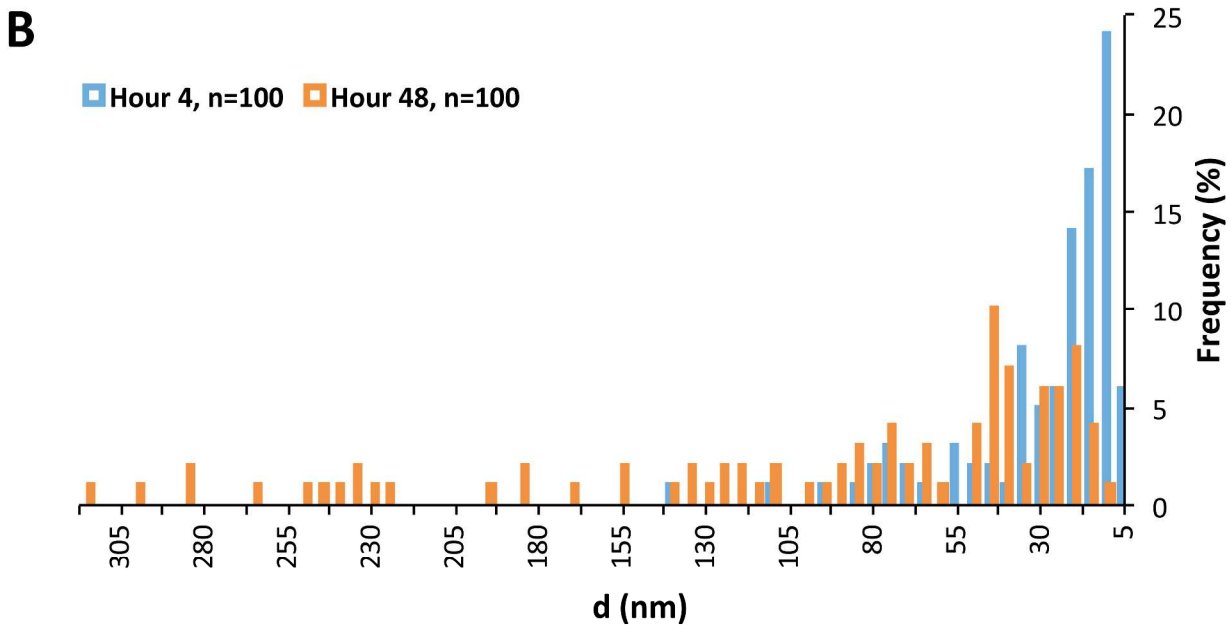

Figure 4 C:

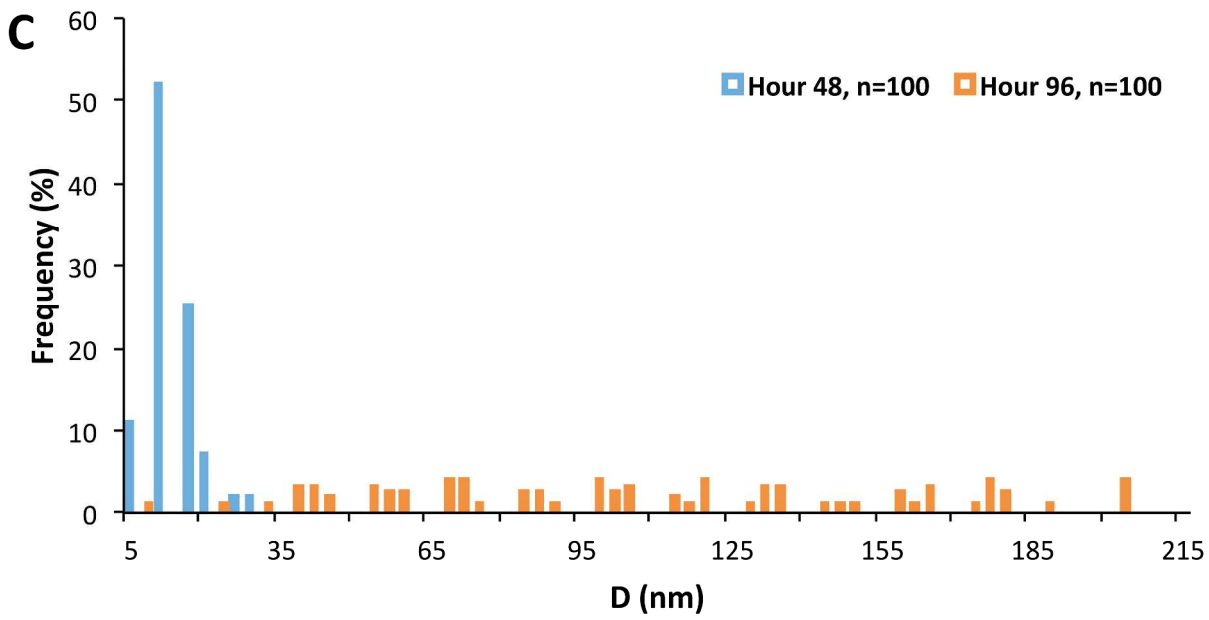

Figure 4 D:

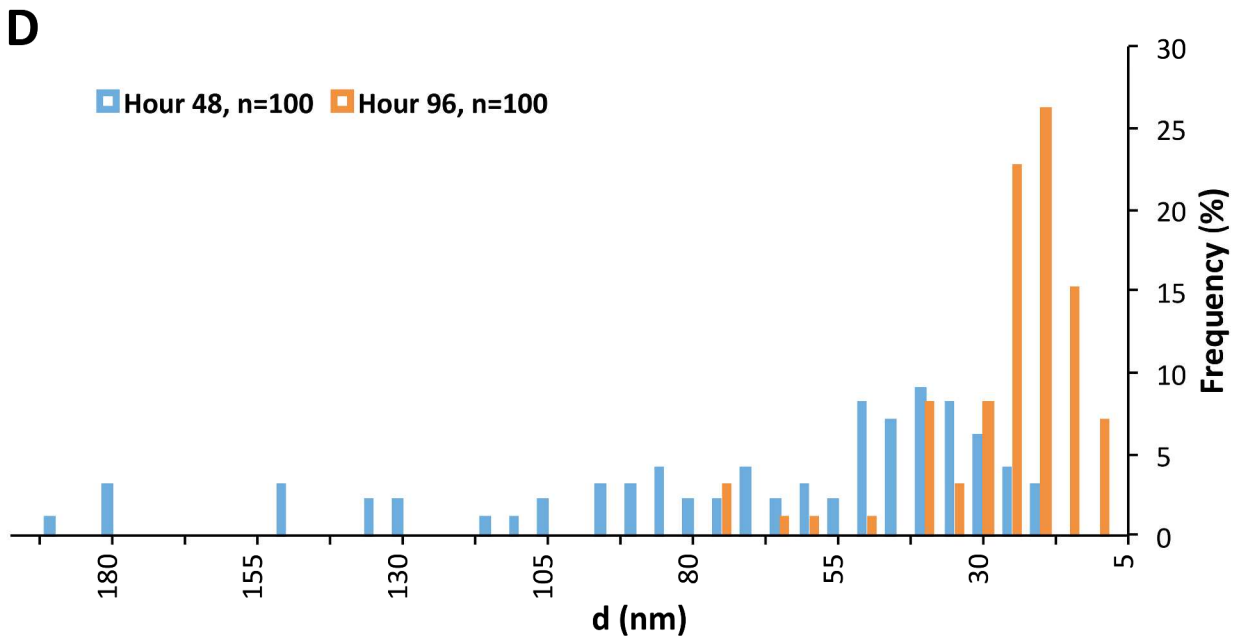

Figure 4 Inset:

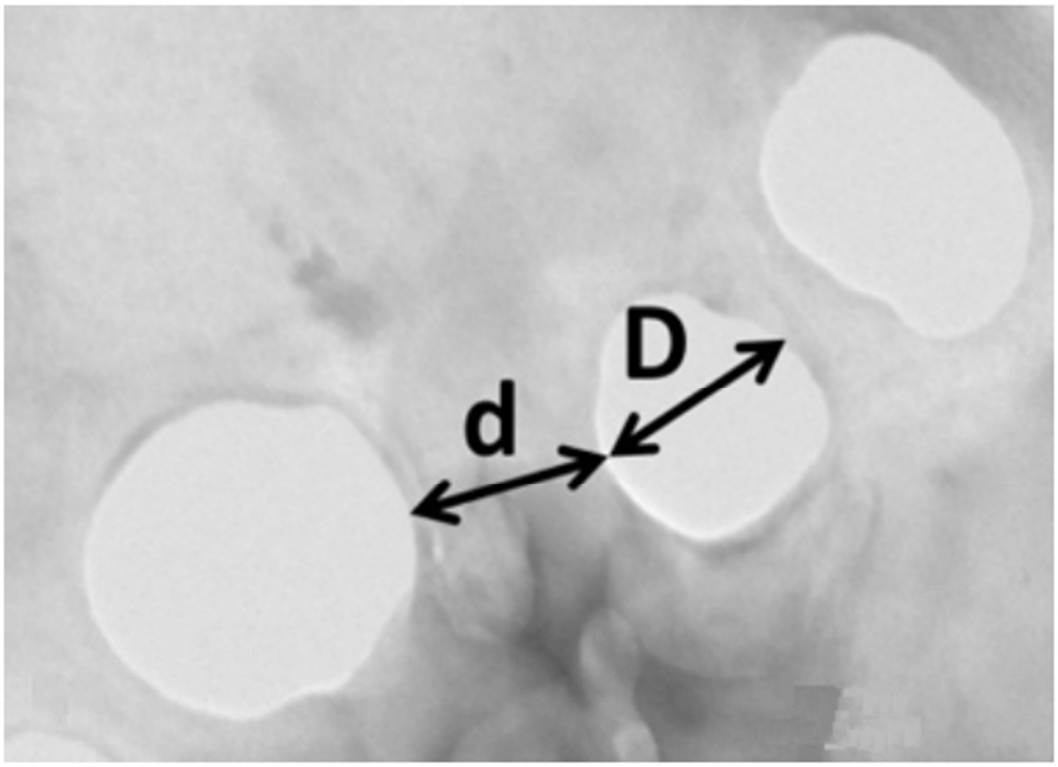

Figure 5 A:

Figure 5 B:

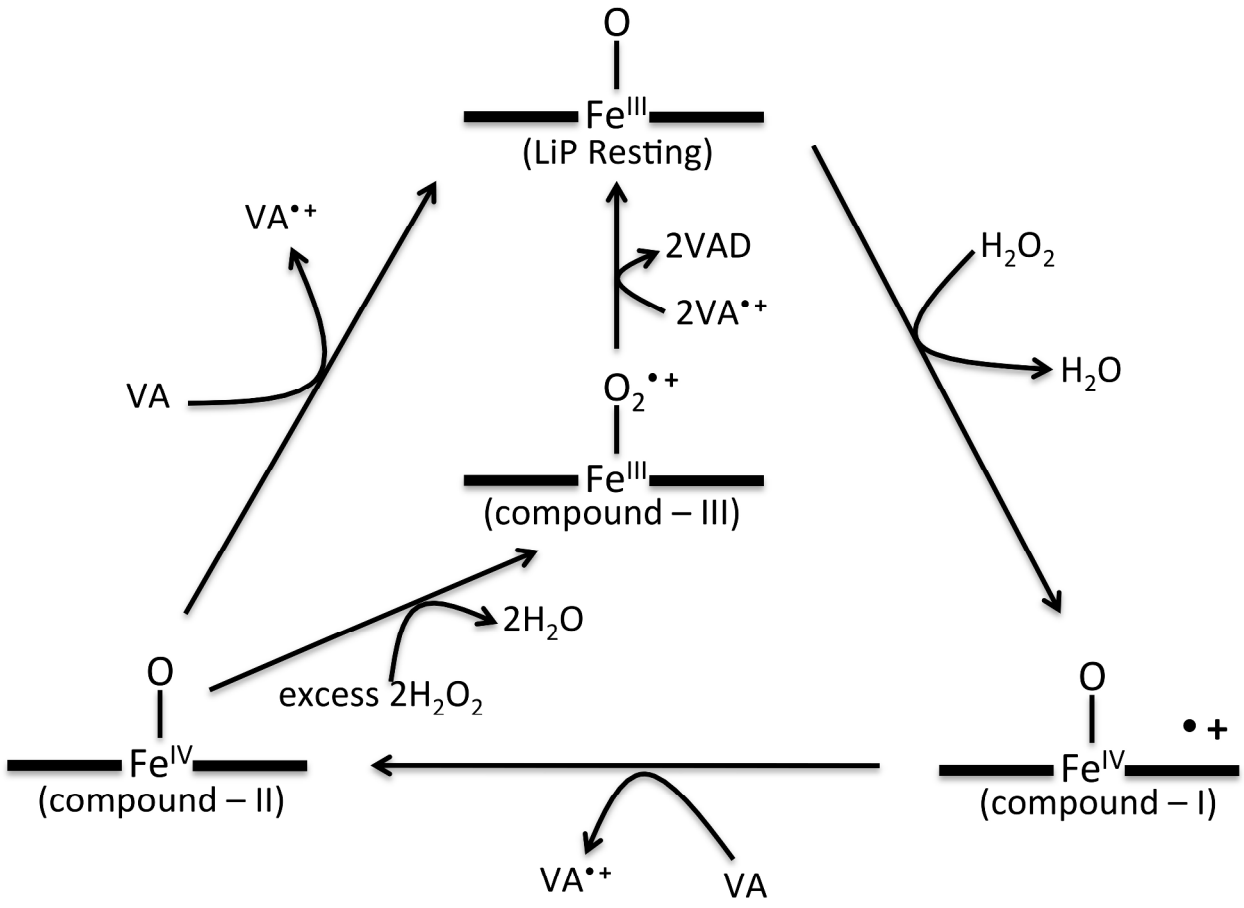

Figure 5 C: